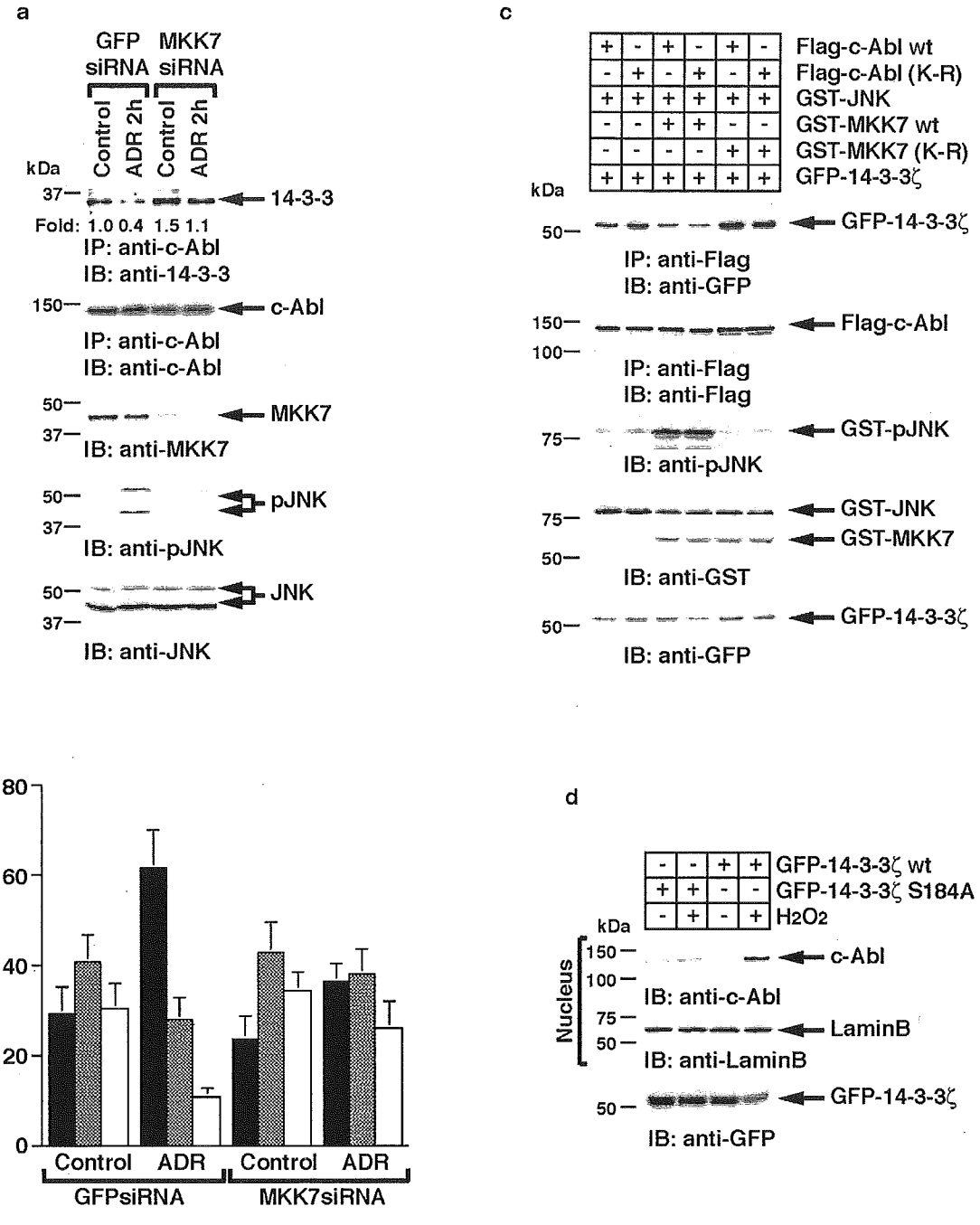

Figure S3 c-Abl-14-3-3 complexes are disrupted by activation of JNK. (a) HeLa cells were transfected with GFPsiRNA or MKK7siRNA. Cell lysates were subjected to immunoprecipitation with anti-c-Abl. The immunoprecipitates were analyzed by immunoblotting with anti-14-3-3 (top panel) or anti-c-Abl (second panel). Lysates were also subjected to immunoblot analysis with anti-MKK7 (third panel), anti-phospho-JNK (fourth panel) or anti-JNK (bottom panel) (b) HeLa cells were treated as in (a). Localization of c-Abl was quantitated as described in the legends to Fig. 3e. (c) 293T cells were transfected as indicated. After 48 h post-transfection, cell lysates were immunoprecipitated with anti-Flag. The immunoprecipitates were then subjected to immunoblot analysis with anti-GFP (top panel) or anti-Flag (second panel). Lysates were also analyzed by immunoblotting with anti-GST (third panel) or anti-GFP (bottom panel). (d) 293T cells were transfected with GFP-14-3-3ζ wt or the S184A mutant. After treatment with 50 μM H_2O_2 for 2 h, nuclear lysates were prepared and analyzed by immunoblotting with anti-c-Abl (upper panel) or anti-LaminB (middle panel). Whole cell lysates were subjected to immunoblot analysis with anti-GFP (lower panel).

STAT3 regulates Nemo-like kinase by mediating its interaction with IL-6-stimulated TGFβ-activated kinase 1 for STAT3 Ser-727 phosphorylation

Hirotada Kojima*, Takanori Sasaki*, Tohru Ishitani†, Shun-ichiro Iemura‡, Hong Zhao*, Shuhei Kaneko*, Hiroyuki Kunimoto*, Tohru Natsume‡, Kunihiro Matsumoto†, and Koichi Nakajima*§

*Department of Immunology, Osaka City University Graduate School of Medicine, 1-4-3 Asahi-machi, Abeno-ku, Osaka 545-8585, Japan; †Department of Molecular Biology, Graduate School of Science, Nagoya University, Chigusa-ku, Nagoya 464-8603, Japan; and ‡National Institutes of Advanced Industrial Science and Technology, Biological Information Research Center, Kohtoh-ku, Tokyo 135-0064, Japan

Communicated by Tadamitsu Kishimoto, Osaka University, Osaka, Japan, January 26, 2005 (received for review November 24, 2004)

Signal transducer and activator of transcription 3 (STAT3) is activated by the IL-6 family of cytokines and growth factors. STAT3 requires phosphorylation on Ser-727, in addition to tyrosine phosphorylation on Tyr-705, to be transcriptionally active. In IL-6 signaling, the two major pathways that derive from the YXXQ and the YSTV motifs of gp130 cause Ser-727 phosphorylation. Here, we show that TGF-β-activated kinase 1 (TAK1) interacts with STAT3, that the TAK1-Nemo-like kinase (NLK) pathway is efficiently activated by IL-6 through the YXXQ motif, and that this is the YXXQ-mediated H7-sensitive pathway that leads to STAT3 Ser-727 phosphorylation. Because NLK was recently shown to interact with STAT3, we explored the role of STAT3 in activating this pathway. Depletion of STAT3 diminished the IL-6-induced NLK activation by >80% without inhibiting IL-6-induced TAK1 activation or its nuclear entry. We found that STAT3 functioned as a scaffold for TAK1 and NLK *in vivo* through a region in its carboxyl terminus. Furthermore, the expression of the $STAT3_{534-770}$ region in the nuclei of STAT3-knockdown cells enhanced the IL-6-induced NLK activation in a dose-dependent manner but not the TGFβ-induced NLK activation. TGFβ did not cause STAT3 Ser-727 phosphorylation, even when the carboxyl region of STAT3 was expressed in the nuclei. Together, these results indicate that STAT3 enhances the efficiency of its own Ser-727 phosphorylation by acting as a scaffold for the TAK1-NLK kinases, specifically in the YXXQ motif-derived pathway.

gp130 | YXXQ motif | signaling specificity

The signal transducer and activator of transcription (STAT) family plays pivotal roles in a variety of systems and in development, in response to cytokines and growth factors. STAT family members are activated in the cytoplasm by tyrosine phosphorylation, form dimers, and enter the nucleus, where they act as DNA-binding transcription factors (1). Of the seven known STATs, STAT1, 3, 5A, 5B, and 6 are phosphorylated at one or two serine residues in their carboxyl-terminal transactivation domain (1, 2) and at a critical tyrosine. The serine phosphorylation enhances the transcriptional activity in the case of STAT1 (3), STAT3 (3, 4), and STAT6 (5). STAT3 can be activated by a variety of cytokines, including the IL-6 family, by using gp130 as a common receptor subunit (6), Granulocyte colony-stimulating factor (G-CSF) and erythropoietin, and growth factors, EGF, platelet-derived growth factor, and hepatocyte growth factor, and cytoplasmic tyrosine kinases, including Src and v-Eyk (reviewed in ref. 7). IL-6 uses STAT3 in its major signaling pathway and concomitantly activates the Ras/Raf/ERK and PI3-kinase pathways (7). IL-6, therefore, activates multiple genes, including acute-phase reactants, and the *junB*, *tis11*, *stat3*, c-*myc*, and c-*fos* genes, mostly through STAT3 (8–14). In the IL-6 receptor system, the tyrosine-phosphorylated YXXQ motif of gp130 is critical for recruiting STAT3 for subsequent phosphorylation at Tyr-705 by the associated Jak kinases (15). In addition, Abe *et al.* (4) showed that the YXXQ motif has another important role in activating STAT3, by phosphorylating Ser-727 through an H7-sensitive kinase pathway in response to IL-6, even at low concentrations. At higher concentrations of IL-6, another PD98059-sensitive pathway derived from the YSTV motif of gp130 also participates in STAT3 Ser-727 phosphorylation (4).

TGF-β-activated kinase 1 (TAK1) is a mitogen-activated protein MAP kinase kinase kinase that is activated by the TGFβ family, IL-1β, TNFα, and the Toll-like receptor family (16–19). TAK1 works with TAB1 (17), TAB2 (20), and TAB3 (21–23) to activate downstream kinases, including the IκB kinases, leading to NF-κB activation, and MAP kinase kinase (MKK) 3/6 and MKK4/7, leading, respectively, to p38 and JNK activation (16, 18, 24, 25). Recently, TAK1 was shown to activate Nemo-like kinase (NLK) in TGFβ (26), Wnt5a (27), and Wnt1 (28) signaling. More recently, Ohkawara *et al.* (29) showed that the TAK1-NLK pathway plays a critical role in TGFβ-induced mesodermal development in *Xenopus* embryos by phosphorylating STAT3 at Ser-727. However, it remains unclear how TAK1 and NLK select their downstream targets in the different signaling pathways.

In this study, we identified TAK1 in the STAT3 complex by using a combination of tandem affinity purification (TAP) and MS. We then found that TAK1 and its downstream kinase, NLK, were selectively activated by IL-6 through the YXXQ motif of gp130. We showed that TAK1 and NLK are critical components of the YXXQ-derived H7-sensitive kinase pathway leading to STAT3 Ser-727 phosphorylation. We further showed that STAT3 specifically enhances the IL-6-induced TAK1-dependent NLK activation, but not TGFβ-induced NLK activation, by acting as a specific scaffold for the kinases involved in the IL-6 signaling. Thus, the upstream TAK1, which is differentially activated by different signaling pathways, seems to select its specific downstream effector kinases in conjunction with a specific scaffold protein, which is STAT3 in the case of the IL-6 signal.

Methods

Cytokines, Abs, and Reagents. The recombinant human IL-6 and G-CSF were gifts from Ajinomoto (Kawasaki, Japan) and Kirin Brewery (Tokyo), respectively. All other cytokines were from PeproTech (London). Rabbit anti-STAT3 and anti-TAK1 Abs were described (18, 30). Anti-phospho-Ser-727 and phospho-Tyr-705 STAT3 Abs were from Cell Signaling Technology (Beverly, MA). Rabbit anti-GST Ab was from Upstate Biotech-

Abbreviations: STAT, signal transducer and activator of transcription; TAK1, TGF-β-activated kinase 1; NLK, Nemo-like kinase; RNAi, RNA interference; TAP, tandem affinity purification; G-CSF; granulocyte colony-stimulating factor; MAP, mitogen-activated protein; MKK; MAP kinase kinase; HA, hemagglutinin; WCE, whole-cell extract; LV, lentivirus.

§To whom correspondence should be addressed. E-mail: knakajima@med.osaka-cu.ac.jp.

www.pnas.org/cgi/doi/10.1073/pnas.0500679102

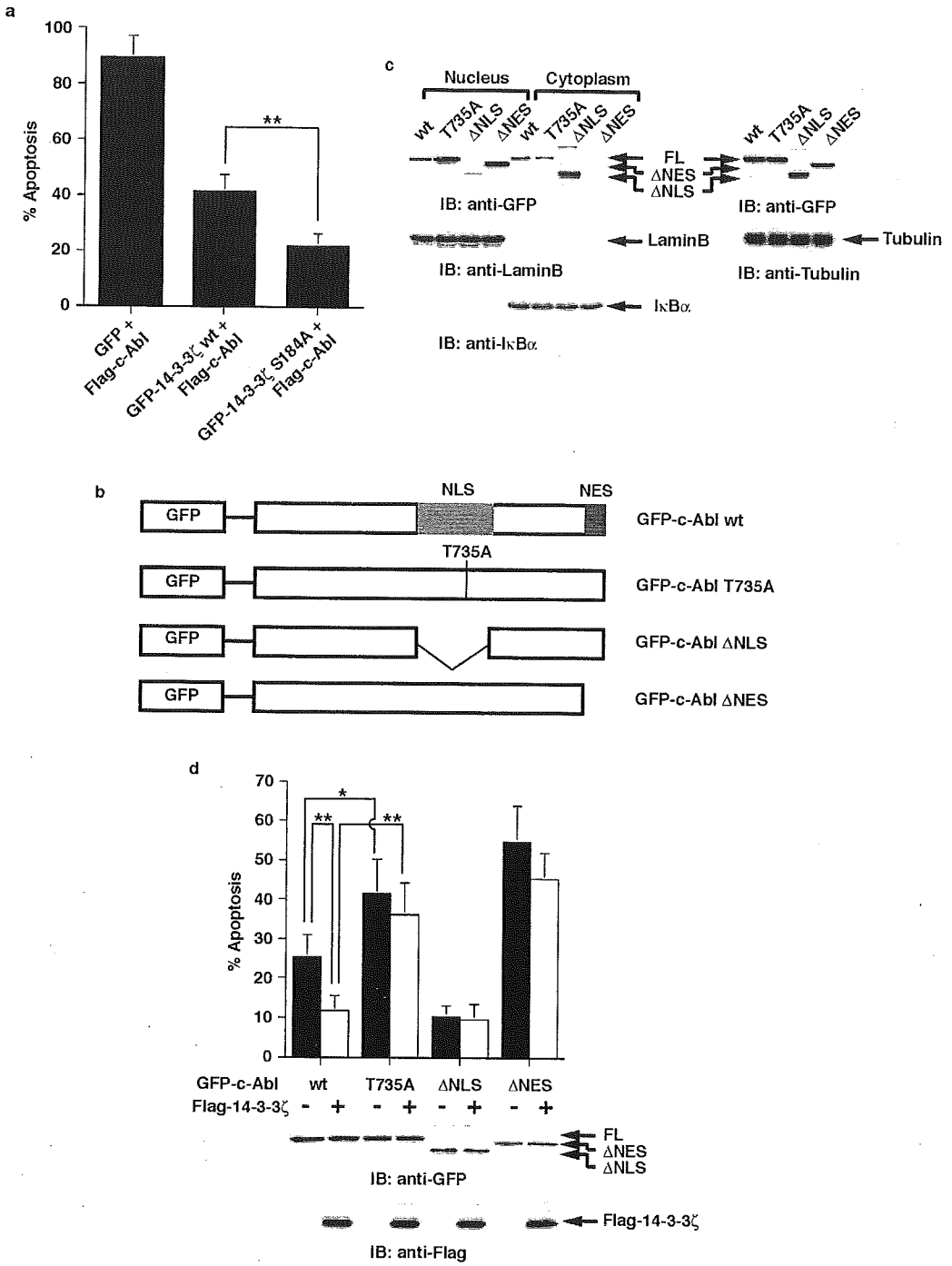

Figure S4 Nuclear targeting of c-Abl is required for the induction of apoptosis. (a) 293T cells were transfected with Flag-c-Abl and GFP vector, GFP-14-3-3ζ wt or S184A mutant. At 24 h post-transfection, cells were treated with 200 μM H_2O_2 for 8 h. DNA content in cells positive for green fluorescence was analyzed by FACscan. The results (mean ± S.D. of eight independent experiments) are represented as the percentage of apoptotic cells with sub-G1 DNA. (b) Constructs of GFP-fused c-Abl and the indicated mutants. (c) 293T cells were transfected with various GFP-c-Abl constructs shown in (b). Nuclear and cytoplasmic lysates were subjected to immunoblot analysis with anti-GFP (left, upper panel), anti-LaminB (left, middle panel) or anti-IκBα (left, lower panel). Whole cell lysates were analyzed by immunoblotting with anti-GFP (right, upper panel) or anti-Tubulin (right, lower panel). (d) 293T cells were co-transfected with the indicated GFP-c-Abl constructs in the presence and absence of Flag-14-3-3ζ. DNA content in cells positive for green fluorescence was analyzed by FACscan. The results (mean ± S.D. of three independent experiments) are represented as the percentage of apoptotic cells with sub-G1 DNA. Cell lysates were subjected to immunoblot analysis with anti-GFP (upper panel) or anti-Flag (lower panel).

nology (Lake Placid, NY). Anti-HA Mo Ab (12CA5) was from Boehringer Mannheim (Mannheim, Germany). All other Abs were from Santa Cruz Biotechnology. H7, 1-(5-iso-quinolinylsulfonyl)-2-methylpiperazine, and all other reagents were from Sigma-Aldrich (St. Louis).

Cell Lines. All of the cell lines were grown in DMEM supplemented with 10% FCS and the appropriate antibiotics. HepG2-G108YRHQ and HepG2-G108YSTV were described (4). The HepG2 cell line with knocked-down *stat3* mRNA (HepG2-STAT3KD) and its derivative cell line with RNA interference (RNAi)-resistant STAT3 (HepG2-KD-STAT3R) were described (14). For the kinase assays, HepG2 cells were cultured in DMEM containing 0.5% FCS for 36 h before stimulation.

Plasmids. The expression vectors encoding the hemagglutinin (HA)-STAT3 and HA-TAK1 were described (18, 31). The TAP tag was attached to the amino terminus of mouse STAT3 (ref. 32 and modified by K.N.), and the TAP-Stat3 cDNA was inserted into the pEF-BOS expression vector (a gift from S. Nagata, Osaka University, Osaka). pCMV-Myc-NLK was generated by inserting a PCR-generated cDNA encoding human NLK into pCDNAMyc (a gift from K. Iwai, Osaka City University, Osaka). For the lentivirus (LV)-mediated expression system, the Myc-NLK cDNA was subcloned into a pCSII-EF-MCS-IRES2-Venus vector (a gift from H. Miyoshi, RIKEN, Tsukuba, Japan). A cDNA fragment encoding $STAT3_{534-770}$ was made by PCR and fused to NLS-FLAG at the amino terminus, and the resultant cDNA was subcloned into the pCSII-EF-MCS-IRES2-Venus vector. All constructs were verified by DNA sequencing. pEF-GST and pEF-GST-$STAT3_{533-770}$ were described (4).

TAP and MS Analysis. TAP was performed as described (32). Briefly, TAP-STAT3 was stably expressed in 293T-G133 cells. Protein complexes interacting with STAT3 were then sequentially affinity-purified by using IgG-Sepharose, Tobacco etch virus protease digestion, and calmodulin beads. The eluates of calmodulin beads were digested with trypsin, and the resultant peptides were subjected to splitless nanoflow liquid chromatography coupled to nanoelectrospray tandem MS (33).

EMSA. ^{32}P-labeled oligonucleotides containing an NF-κB-binding site (5′-AGTGAGGGGACTTTCCGAGTG-3′) from the intercellular adhesion molecule-1 promoter and nuclear extracts from HepG2 cells were used.

LV-Mediated Expression of RNAi. We generated RNAi constructs in the plasmid pU6i-cassette (Genofunction) (34). The target positions of the RNAi against human TAK1 and human NLK were as follows: TAK1, GAGATCGACTACAAGGAGA; NLK, GGCGCACCATCATCAGCAC. To construct the lentiviral RNAi expression system, the cassette containing the U6 promoter and the RNAi was transferred into an LV vector, CS-RfA-EG, with the EF1α promoter-driven GFP gene (a gift from H. Miyoshi). LVs were prepared according to the previously described method (35), except that a three-vector system was used instead of a four-vector system (36).

***In Vitro* Kinase Assay.** The *in vitro* kinase assays were performed as described (26). For the TAK1 kinase assays, endogenous TAK1 was used, and in some experiments, transiently expressed Flag-tagged TAK1 was used, with recombinant MKK6 from *Escherichia coli* as a substrate. For the NLK kinase assays, Myc-tagged NLK protein was extracted from various HepG2 cell lines expressing Myc-NLK, and subjected to the *in vitro* kinase assay to detect autophosphorylation. In some experiments, GST-$STAT3_{534-770}$ produced in *E. coli* was used as a substrate.

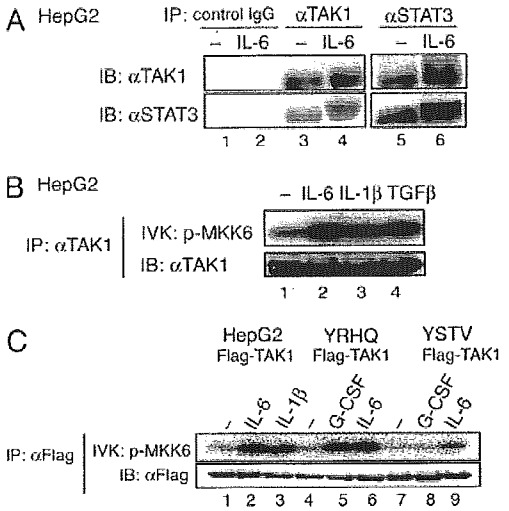

Fig. 1. Endogenous TAK1 binds to STAT3 and is activated through the YXXQ motif in gp130. (*A*) HepG2 cells were untreated (–) or treated with IL-6 for 15 min. WCE was immunoprecipitated (IP) with control IgG (lane 1–2), anti-TAK1 (lanes 3 and 4), or anti-STAT3 (lanes 5 and 6) Abs. Immunoprecipitates were resolved on SDS/PAGE and immunoblotted (IB) with the indicated Abs. (*B*) HepG2 cells were untreated (–) or treated with 20 ng/ml IL-6, IL-1β, or TGF-β for 10 min. The proteins immunoprecipitated with anti-TAK1 Ab were divided into two aliquots. One aliquot was subjected to an *in vitro* kinase assay (IVK) with recombinant MKK6 as the substrate (*Upper*), and the other aliquot was used in an immunoblot to examine the amount of immunoprecipitated TAK1 (*Lower*). (*C*) HepG2, HepG2-G108-YRHQ, or HepG2-G108-YSTV cells were transfected with pEF-Flag-TAK1 plasmid, and untreated (–) or treated with the indicated cytokines at 20 ng/ml for 10 min. The anti-Flag immunoprecipitates of WCEs were subjected to the kinase assay (*Upper*) and immunoblot analysis with an anti-Flag Ab (*Lower*) as in *B*.

Results

Identification of TAK1 as a STAT3-Interacting Protein That Is Activated by IL-6 Through the YXXQ Motif in gp130. To identify molecules acting with STAT3, we first obtained STAT3-associated complexes by the TAP method (32) from gp130-stimulated 293T-G133 cells (4) stably expressing TAP-tagged STAT3. We analyzed digests of the complexes by using direct nanoflow liquid chromatography-coupled tandem MS (33) and identified multiple peptides. One peptide sequence, QELVAELDQDEK, corresponded to residues 521–532 of human TAK1. We then tested whether endogenous TAK1 and STAT3 formed complexes in HepG2 cells. As shown in Fig. 1*A*, lanes 3 and 4, anti-TAK1 immunoprecipitates of WCEs from unstimulated and IL-6-stimulated HepG2 cells contained STAT3. The STAT3–TAK1 interaction was reciprocally confirmed by detecting TAK1 in the anti-STAT3 immunoprecipitates (Fig. 1*A*, lanes 5 and 6).

We next tested whether IL-6 could activate endogenous TAK1. Anti-TAK1 immunoprecipitates of WCEs from unstimulated or IL-6-stimulated HepG2 cells were subjected to an *in vitro* kinase assay by using MKK6 as the substrate. As shown in Fig. 1*B*, IL-6 activated endogenous TAK1 as efficiently as did IL-1β and TGFβ. We next tested whether a tyrosine-phosphorylated motif in gp130 was required for TAK1 activation. As shown in Fig. 1*C*, stimulation of HepG2-G108YRHQ cells that express a chimeric receptor consisting of G-CSFR-gp130 with the cytoplasmic portion of gp130 truncated to 108 amino acid residues and a YXXQ motif peptide, efficiently increased the TAK1 kinase activity. In contrast, this increase was not seen in HepG2-G108YSTV cells that contain a YSTV motif instead of the YXXQ motif. These results indicated that the YXXQ motif was responsible for the TAK1 activation.

IMMUNOLOGY

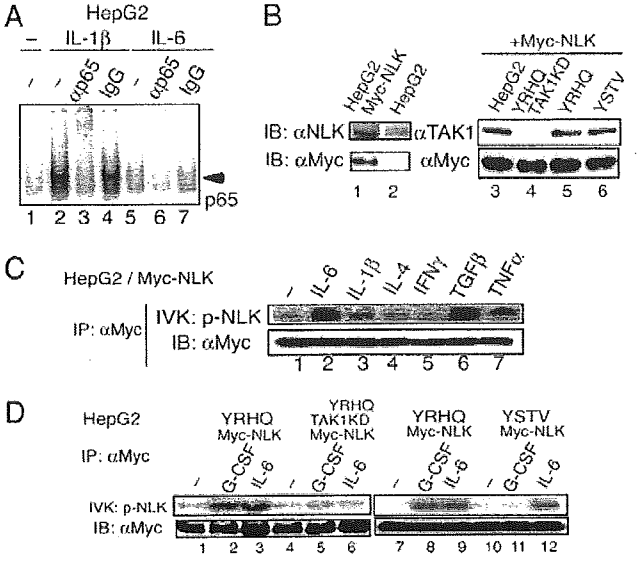

Fig. 2. Preferential activation of NLK through the YXXQ-TAK1 pathway. (*A*) EMSA for NFκB activity. ^{32}P-labeled oligonucleotides containing an NFκB-binding site and nuclear extracts from HepG2 cells that were untreated (–) or stimulated with IL-1β or IL-6 for 30 min were used. The reaction mixtures were preincubated with no additions (lanes 1, 2, and 5), anti-p65 Ab (lanes 3 and 6), or control rabbit IgG (lanes 4 and 7). (*B*) HepG2 cells (lanes 1 and 3), HepG2-G108YRHQ (lane 5), HepG2-G108YSTV (lane 6), or HepG2-G108YRHQ with TAK1 KD (lane 4, see also Fig. 3*A*) cells were infected with LV-Myc-NLK. WCEs from parental (lane 2) and the transfected cells were immunoblotted (IB) with an anti-NLK Ab (*Left Upper*, lanes 1 and 2), an anti-TAK1 Ab (*Right Upper*, lanes 3–6) or anti-Myc Ab (*Lower*). The total amount of endogenous and exogenous NLK in the HepG2-Myc-NLK cells was estimated as ≈2- to 2.2-fold of that of endogenous NLK in the parental cells. (*C* and *D*) The various HepG2-Myc-NLK cells shown in *B* were left unstimulated or stimulated with the indicated cytokines at 20 ng/ml for 10 min. The anti-Myc immunoprecipitates (IP) of WCE were divided into two aliquots. Each aliquot was subjected to the NLK kinase assay in the absence of exogenous substrate (*Upper*) or immunoblot analysis with the anti-Myc Ab (*Lower*).

IL-6 Preferentially Activates NLK Via the YXXQ-TAK1-Mediated Pathway. Once we discovered that IL-6 activated TAK1, we investigated which downstream pathways were activated through TAK1 in response to IL-6. First, we examined NFκB activation by using an EMSA. In contrast to the efficient induction of NFκB containing p65 by IL-1β (Fig. 2*A*, lanes 2 and 3), IL-6 caused only slight NFκB DNA-binding activity in HepG2 cells (Fig. 2*A*, lanes 5 and 6). p38 and JNK activation were also tested, with no apparent activation observed in the IL-6-stimulated HepG2 cells (data not shown). We then examined whether IL-6 activated NLK. To efficiently test the NLK kinase activity, we stably expressed Myc-tagged NLK (Myc-NLK) in HepG2 cells, HepG2-G108YRHQ, or HepG2-G108YSTV, and a HepG2 cell line in which TAK1 was knocked down (described later and shown in Fig. 3*A*), with an LV expression system. The expression levels of Myc-NLK were very similar in these cell lines (Fig. 2*B*, lanes 3–6), and the level of Myc-NLK was close to that of endogenous NLK in HepG2 cells (Fig. 2*B*, lanes 1 and 2). The Myc-NLK was recovered with an anti-Myc Ab from HepG2 cells that had either been left unstimulated or stimulated, as indicated, for 10 min. The Myc-NLK was then tested for its autophosphorylation kinase activity (Fig. 2*C*). IL-6 activated NLK efficiently, as did TGFβ, IL-1β, and TNFα; two other cytokines, IFNγ and IL-4, did not activate NLK. Consistent with the role played by the YXXQ motif in the IL-6-induced TAK1 activation, stimulation of the chimeric GCSF-R-gp130 receptor containing the YXXQ motif, but not the YSTV motif, caused NLK activation at the level similar to that obtained with IL-6 (Fig. 2*D*, lanes 1–3 and 7–12). Together with the finding that the YXXQ-derived signal-induced and IL-6-induced NLK activation was severely impaired in TAK1-knockdown HepG2 cells (Fig. 2*D*, lanes 4–6), these results indicated that IL-6 preferentially activates the TAK1-NLK pathway through the YXXQ motif.

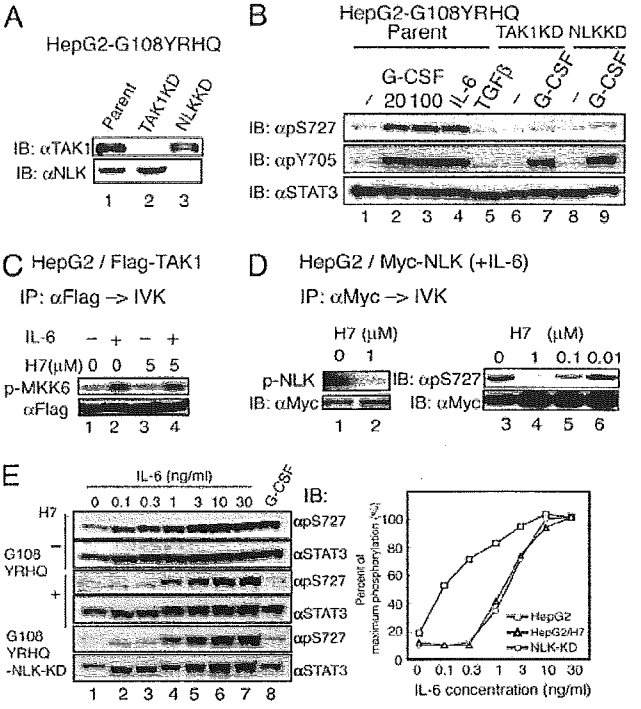

Fig. 3. TAK1 and NLK are components of the YXXQ-mediated H7-sensitive kinase pathway leading to the phosphorylation of STAT3 Ser-727. (*A*) HepG2-G108YRHQ cells were infected with LV-U6-small interfering RNA against TAK1 and NLK to deplete TAK1 and NLK (TAK1KD and NLKKD, respectively). The silencing effect was evaluated by immunoblotting with the indicated Ab. (*B*) HepG2-G108YRHQ cells and the TAK1KD or NLK KD HepG2-G108YRHQ cells were left unstimulated or stimulated with the indicated cytokines at 20 ng/ml (lanes 2, 4, and 5) or at 100 ng/ml (lanes 3, 7, and 9) for 15 min. The WCEs were immunoblotted with the indicated Abs. (*C*) The Flag-TAK1 immunoprecipitates from unstimulated or IL-6-stimulated HepG2 cells were subjected to the *in vitro* kinase assay as in Fig. 1*B* in the absence or presence of 5 μM H7. (*D*) HepG2-Myc-NLK cells were stimulated with IL-6 at 20 ng/ml for 15 min. The immunoprecipitates of WCEs with anti-Myc Ab were subjected to the *in vitro* NLK kinase assay as in Fig. 2*C* (lanes 1 and 2) or the *in vitro* NLK kinase assay by using GST-STAT3 (534–770) made in *E. coli* (lanes 3–6) in the presence of the indicated amounts of H7. Phospho-Ser-727 was detected with an anti-phospho-Ser-727 Ab (*Right Upper*). The amount of NLK used for each kinase assay is shown in *Lower*. (*E*) HepG2-G108YRHQ cells pretreated with nothing (–) or H7 at 50 μM (+) and HepG2-G108YRHQ-NLK-KD cells were left unstimulated or stimulated with the indicated concentrations of IL-6 (lanes 2–7) or 20 ng/ml G-CSF for 15 min. The WCEs were immunoblotted with the indicated Abs (*Left*). The intensities of each band were quantified by a densitometer (GS-700, Bio-Rad), and the percentage of STAT3 in the phosphorylated form was calculated (*Right*). The value in HepG2 cells stimulated with 30 ng/ml IL-6 was defined as 100%, because almost all of the STAT3 was phosphorylated on Ser-727, as judged by its migration pattern on SDS/PAGE (data not shown). Average values of two independent experiments are shown.

The TAK1-NLK Pathway Is the YXXQ-Mediated H7-Sensitive Pathway That Leads to STAT3 Ser-727 Phosphorylation. To test the roles of endogenous TAK1 and NLK in the IL-6- and YXXQ-derived signaling, we knocked down the expression levels of TAK1 or NLK in HepG2-G108YRHQ cells by the RNAi method, using a

lentiviral vector system expressing a U6-driven loop-type small interfering RNAs against the *tak1* and *nlk* mRNAs. The LV without an RNAi sequence was used as the control. The small interfering RNAs against the *tak1* and *nlk* mRNAs effectively inhibited the production of their corresponding proteins (Fig. 3*A*). As shown in Fig. 3*B*, the YXXQ signal efficiently caused Ser-727 phosphorylation as did IL-6 at 20 ng/ml, and the YXXQ-mediated Ser-727 phosphorylation was severely impaired in both the TAK1- and NLK-depleted cells, whereas the phosphorylation of STAT3 on Tyr-705 was intact in these cells, indicating that the TAK1-NLK pathway is critical for STAT3 Ser-727 phosphorylation by the YXXQ-derived pathway. It was also noted that TGFβ did not cause STAT3 Ser-727 phosphorylation in HepG2 cells despite the strong NLK activation (Fig. 3*B*, lane 5). TAK1 kinase activity was resistant to H7 at 5 μM in the *in vitro* kinase assay (Fig. 3*C*, lanes 3 and 4), whereas the NLK kinase activity was very sensitive to H7 in the autophosphorylation kinase assay (Fig. 3*D*, lanes 1 and 2), and in an assay using GST-STAT3$_{534-770}$ made in *E. coli* as the substrate (Fig. 3*D*, lanes 3–6) with an of IC_{50} <0.1 μM. We then tested the role of this pathway in STAT3 Ser-727 phosphorylation at various IL-6 concentrations. We compared the levels of STAT3 Ser-727 phosphorylation in HepG2-G108YRHQ cells and NLK-knockdown-HepG2-G108YRHQ cells in response to increasing doses of IL-6. As shown in Fig. 3*E*, STAT3 Ser-727 phosphorylation by IL-6 was detected even at 0.1 ng/ml IL-6 and peaked at ≈10 ng/ml in the parental cells. In contrast, in the NLK-KD cells, the Ser-727 phosphorylation responses were suppressed when stimulated with 0.1, 0.3, and 1 ng/ml IL-6, but gradually reached a maximal level similar to that seen in the parental cells at 10 ng/ml. Very similar responses were observed in HepG2 cells pretreated with H7 at 50 μM (Fig. 3*E*, indicated as H7+) and in the HepG2-G108-TAK1KD cells (data not shown). These results indicated that the TAK1-NLK pathway actually represented the components of the previously characterized YXXQ-derived H7-sensitive kinase pathway that leads to STAT3 Ser-727 phosphorylation.

STAT3 Is Required for IL-6-Induced NLK Activation but Not for TAK1 Activation. Because STAT3 interacts with TAK1 even after IL-6 stimulation (Fig. 1*A*) and with NLK (29), we explored the role of STAT3 in the YXXQ-derived TAK1-NLK pathway. We used STAT3-knockdown HepG2 cells (HepG2-STAT3KD) and a derivative HepG2-STAT3KD cell line that was reconstituted with short interfering RNA-resistant STAT3 (HepG2-KD-STAT3R) (14). Stimulation with IL-6 at 1 and 100 ng/ml caused TAK1 activation in the HepG2-STAT3KD cells to levels comparable to those obtained in the parental cells (Fig. 4*A*, lanes 1–6). Interestingly, in response to IL-6, TAK1 translocated into the nucleus (Fig. 6*A*, which is published as supporting information on the PNAS web site), and the kinase activities in both the cytosolic and nuclear fractions increased even without STAT3 (Fig. 4*A*, lanes 7–14). These results indicated that the presence of STAT3 did not affect the activation step of TAK1 in response to IL-6.

In contrast, the IL-6-induced NLK kinase activity was markedly reduced in the HepG2-STAT3KD cells, to <20% of the activity obtained with the parental cells (Fig. 4*B*, lanes 2 and 6; see also Fig. 5*C*; average = 17.6 ± 7.2%, n = 4), and this IL-6-induced NLK activity fully recovered in the HepG2-KD-STAT3R cells (Fig. 4*B*, lanes 9 and 10), suggesting that STAT3 has a role in the TAK1-dependent NLK activation after the TAK1 activation step of the IL-6 signal. This STAT3-dependency was not observed for the NLK activation by IL-1β or TGFβ (Fig. 4*B*), indicating a specific role for STAT3 in NLK activation by IL-6 signals.

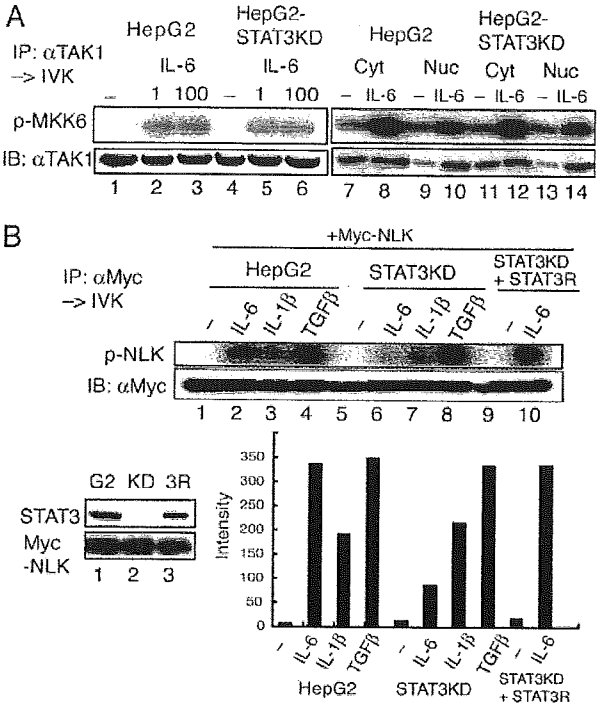

Fig. 4. STAT3 is required for IL-6-induced NLK activation but not for TAK1 activation. (*A*) HepG2 and HepG2-STAT3-knockdown (KD) cells were left unstimulated or stimulated with IL-6 at 1 (lanes 2 and 5), 100 (lanes 3 and 6), or 20 (lanes 8, 10, 12, and 14) ng/ml. Endogenous TAK1 from WCE extracts (lanes 1–6), cytosolic extracts (Cyt, lanes 7, 8, 11, and 12) or nuclear extracts (Nuc, lanes 9, 10, 13, and 14) was immunoprecipitated with an anti-TAK1 Ab, and the kinase activity was measured by using MKK6 as the substrate (*Upper*). (*Lower*) Immunoblotting with the anti-TAK1 Ab. (*B*) HepG2 (G2) cells, HepG2-STAT3KD (KD), and HepG2-STAT3KD reconstituted with RNAi-resistant STAT3 (3R) were infected with LV- Myc-NLK. The expression levels of STAT3 and Myc-NLK are shown in *Left Lower*. These HepG2 and derivative cells expressing Myc-NLK were left unstimulated or stimulated with the indicated cytokines at 20 ng/ml for 10 min. Kinase assay (*Upper*) and Western blotting analysis (*Lower*) of the anti-Myc-immunoprecipitates of WCE are shown. The radioactivity level of each band in the kinase assay was quantified with the BAS 5000 Bioimaging analyzer (Fujix, Tokyo). The activity of NLK in the IL-6-stimulated HepG2-STAT3 KD was estimated to be 17.6 ± 7.6% of that of IL-6-stimulated HepG2 cells (n = 4).

STAT3 Enhances the TAK1-Dependent NLK Activation by Acting as a Scaffold Specifically in the YXXQ-Derived Signal. We previously showed that the carboxyl-terminal region of STAT3 from residues 533 to 770 was enough to be phosphorylated on Ser-727 by the YXXQ-derived pathway (4). Consistently, GST-STAT3$_{533-770}$ fusion protein interacted with HA-TAK1 or Myc-NLK when coexpressed in 293T cells (data not shown). We then examined the nature of the interactions among STAT3, TAK1, and NLK. Glutathione beads were loaded with WCEs from cells coexpressing GST or GST-STAT3$_{533-770}$, Myc-NLK, and HA-TAK1. The protein complexes containing GST and GST-STAT3$_{533-770}$ were then recovered from the beads. As shown in Fig. 5*A*, TAK1, and NLK, interacted with GST-STAT3$_{533-770}$ (lane 4), but not with GST (lane 3). The eluates from the beads were then further immunoprecipitated with an anti-Myc Ab to obtain the NLK complexes. Anti-Myc immunoprecipitates of the eluates contained HA-TAK1 and GST-STAT3$_{533-770}$ in addition to Myc-NLK (lane 6). Control GST did not cause this coimmunoprecipitation (lane 5). Taken together with the fact that TAK1 does not directly interact with NLK (28), these results indicate that STAT3 formed a ternary complex with HA-TAK1 and Myc-NLK through its carboxyl-terminal region.

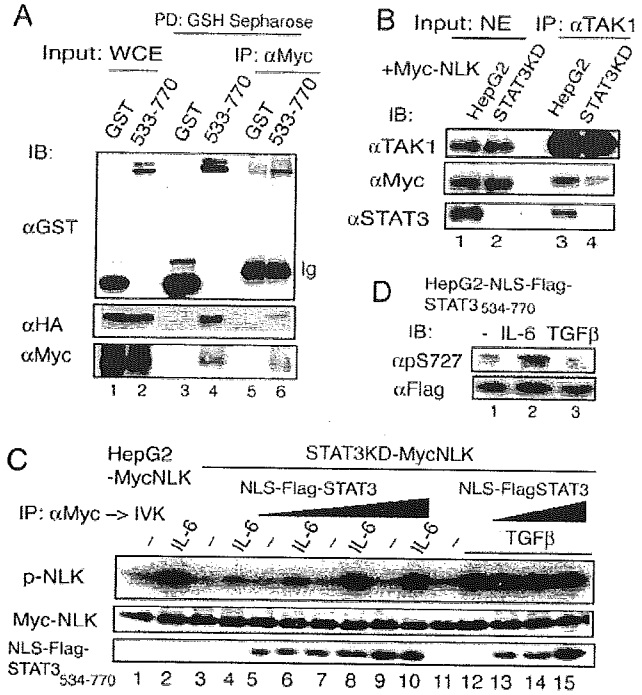

Fig. 5. The STAT3 molecule acts as a scaffold for TAK1/NLK in the YXXQ-derived pathway. (*A*) 293T cells were transfected with pCMV-HA-TAK1, pCMV-Myc-NLK, and pEFGST or pEFGST-STAT3$_{533-770}$ plasmid. The GST-labeled proteins were pulled-down with reduced glutathione (GSH)-Sepharose. The eluates were diluted with 50 mM Hepes buffer (pH 7.8) containing 150 mM NaCl, and subjected to immunoprecipitation using an anti-Myc Ab. The WCEs (lanes 1 and 2), the eluates from the GSH-Sepharose (lanes 3 and 4), and the anti-Myc Ab immunoprecipitates (lanes 5 and 6) were subjected to immunoblotting analysis with the indicated Abs. (*B*) HepG2-MycNLK and HepG2-STAT3KD-MycNLK were treated with 20 ng/ml IL-6 for 10 min. The nuclear extracts (500 μg each) were immunoprecipitated with an anti-TAK1 Ab. Nuclear extracts (20 μg, lanes 1 and 2) and the immunoprecipitates (lanes 3 and 4) were separated and probed with the indicated Abs. (*C*) HepG2-STAT3KD-MycNLK cells were infected with three doses of lentiviral preparation LV-EFNLS-FlagSTAT3$_{534-770}$. HepG2-MycNLK-, HepG2-STAT3KD-MycNLK-, and NLS-FlagSTAT3$_{534-770}$-expressing cells were stimulated with IL-6 (lanes 2, 4, 6, 8, and 10), or TGF-β (lanes 12–15) at 20 ng/ml, for 10 min or left unstimulated. The anti-Myc-immunoprecipitates (IP) of WCEs were subjected to the *in vitro* NLK kinase assay (*p*-NLK) and immunoblot (IB) with the anti-Myc Ab. (*Lower*) Immunoblots using an anti-STAT3 Ab indicate that the lysate samples contained increasing amounts of NLS-FlagSTAT3$_{534-770}$ protein in the WCE. (*D*) HepG2 cells expressing NLS-FlagSTAT3$_{534-770}$ were left untreated or treated with IL-6 or TGFβ for 15 min. The WCEs were separated on SDS/PAGE and probed with the indicated Abs.

Next, we further tested whether the interaction of endogenous TAK1 and NLK in the nucleus required STAT3 molecules. The Myc-NLK, which was expressed at a level similar to that of endogenous NLK, was located largely in the nucleus with or without IL-6 stimulation, as was endogenous NLK (Fig. 6 *B* and *C*). As shown in Fig. 5*B*, lanes 1 and 2, Myc-NLK was present at a similar level in the nuclear extracts from IL-6-stimulated HepG2-MycNLK and HepG2-STAT3KD-MycNLK cells. Comparable amounts of TAK1 were present in the nucleus (Fig. 5*B*, lanes 1 and 2) in response to IL-6, even in the absence of STAT3, and efficiently recovered with an anti-TAK1 Ab (Fig. 5*B*, lanes 3 and 4). NLK and STAT3 clearly coimmunoprecipitated with TAK1 in the nuclear extracts of IL-6-stimulated HepG2-MycNLK cells (Fig. 5*B*, lane 3), whereas the amount of NLK that coimmunoprecipitated with TAK1 in the nuclear extracts of HepG2-STAT3KD-MycNLK cells (Fig. 5*B*, lane 4) was markedly reduced to ≈15% of that in Fig. 5*B*, lane 3. These results indicate that the nuclear TAK1-NLK interaction in response to IL-6 is largely dependent on STAT3.

To substantiate this TAK1–STAT3–NLK interaction, we stably expressed an NLS-FlagSTAT3$_{534-770}$ at three different levels in HepG2-STAT3KD-MycNLK cells. These cells were left unstimulated or stimulated with IL-6 or TGFβ for 10 min, and the NLK activities were assayed. As shown in Fig. 5*C*, expression of the carboxyl terminus of STAT3 in the nucleus enhanced the IL-6-induced NLK activation in a dose-dependent manner. Interestingly, the TGFβ-induced NLK activation was not enhanced by the presence of the carboxyl terminus of STAT3 in the nucleus. These results indicate that STAT3 has an enhancing effect on the TAK1-dependent NLK activation, specifically in IL-6 signaling. We further tested whether NLK that was activated by the TGFβ signal in a STAT3-independent manner could phosphorylate STAT3 on Ser-727 in the nucleus. Very interestingly, in contrast to IL-6, TGFβ did not cause Ser-727 phosphorylation of the NLS-FlagSTAT3$_{534-770}$ expressed in the nucleus (Fig. 5*D*), suggesting that the substrate specificity of the NLKs that are activated through different pathways depends on the scaffold proteins used in the specific signaling pathways.

Discussion

This study showed that gp130, a member of the cytokine receptor superfamily, efficiently activates the TAK1 through the YXXQ motif in gp130, and this kinase preferentially activates the downstream kinase NLK, which is responsible for STAT3 Ser-727 phosphorylation via the YXXQ motif-derived signal. Furthermore, this study revealed a novel role for STAT3 in IL-6-induced NLK activation but not in TGFβ-induced NLK activation. STAT3 functions as a scaffold for TAK1 and NLK specifically in IL-6 signaling by binding them at its carboxyl-terminal region. The following observations support the idea that this interaction is physiologically significant: (*i*) most TAK1-NLK interactions in the nuclear extracts of IL-6-stimulated HepG2 cells depended on the presence of STAT3 (Fig. 5*B*); (*ii*) the IL-6-induced NLK activation was greatly decreased in HepG2-STAT3KD cells; (*iii*) STAT3 and TAK1 were independently activated by IL-6, even at low concentrations, and they then translocated into the nucleus (Figs. 4*B* and 6*A*), although most NLK resides in the nucleus before stimulation (ref. 36 and Fig. 6*B*); and (*iv*) expression of the carboxyl-terminal portion of STAT3 in the nucleus markedly increased the IL-6-induced NLK activation. In contrast, TGFβ neither used STAT3 to activate NLK (Fig. 4*B*) nor caused the phosphorylation of STAT3 on Ser-727 (Fig. 3*B*). This finding could not be explained by the fact that TGFβ did not cause the translocation of STAT3, because TGFβ-induced NLK activation could not be enhanced by the forced expression of STAT3 in the nucleus (Fig. 5*C*), and NLK activated by TGFβ did not cause Ser-727 phosphorylation of the nuclear STAT3 (Fig. 5*D*). Thus, NLKs activated through different pathways have different substrate specificities, probably reflecting the nature of the complexes containing the upstream TAK1 kinase and the scaffold proteins involved in the specific activation signals.

We previously showed that the IL-6 signals for STAT3 Ser-727 phosphorylation are mediated by at least two kinase pathways, one is a YSTV-motif-derived PD98059-sensitive pathway, and the other is a YXXQ-motif-derived H7-sensitive kinase pathway (4). The kinase pathway described here is fully consistent with the H7-sensitive kinase pathway, because it has all of the characteristics previously shown for the YXXQ-derived H7-sensitive kinase that leads to STAT3 Ser-727 phosphorylation, including the characteristics indicated in Fig. 3 *C–E*. This pathway was also active in other cell lines tested, including the NIH 3T3 and HEK293T cell lines (H. Kojima, T.S., and K.N., unpublished data). This pathway seems to be rather specific to

the receptor systems that use gp130 or to others containing the YXXQ motif, because neither IFNγ nor IL-4 activated NLK. Other cytokines should be tested to see if they activate this pathway.

To date, only a few downstream targets of NLK have been identified, including TCF/LEF (26), STAT3 (ref. 29 and this study), and c-Myb (28). We do not know what other NLK substrates are in the YXXQ-derived pathway at present. Recently, Kanei-Ishii *et al.* (28) showed that TAK1, which is activated by the Wnt-1 signal, activates NLK through HIPK2, which functions as an intermediate kinase between TAK1 and NLK. NLK then phosphorylates c-Myb at multiple sites, leading to ubiquitination and proteasome-dependent degradation. In their case, c-Myb interacted with HIPK2 and NLK in the nucleus. It would be intriguing to test whether c-Myb works as a scaffold for NLK activation specifically in Wnt-1 signaling, as STAT3 appears to do in IL-6 signaling. Ohkawara *et al.* (29) showed that the TAK1-NLK pathway is responsible for the phosphorylation of *Xenopus* STAT3 on Ser-727 in the marginal zone of the 32-cell embryo, and that NLK interacts with and phosphorylates STAT3 on Ser-727 *in vitro*. Together with results showing that both STAT3 and TAK1-NLK are required for TGFβ-mediated mesoderm induction, they concluded that the TAK1-NLK-STAT3 cascade participates in the TGFβ-mediated mesoderm induction (29). However, in the present report, TGFβ did not cause STAT3 Ser-727 phosphorylation in HepG2 cells, even when the carboxyl portion of STAT3 was expressed in the nucleus, despite the strong activation of NLK by TGFβ. Clearly, more studies need to be performed to understand how different upstream pathways select the downstream kinases and affect the substrate specificity of those kinases.

We gratefully acknowledge Akihiro Iwamatsu and his laboratory for advice on protein identification. We are indebted to H. Miyoshi for the lentiviral vector system. We thank Y. Niwa for technical assistance and E. L. Barsoumian for encouraging us. This work was supported in part by the Ministry of Education, Culture, Sports, Science, and Technology of Japan, Nippon Boehringer Ingelheim Co., Ltd., GenoFunction, Inc., and the Osaka Foundation for Promotion of Clinical Immunology.

1. Levy, D. E. & Darnell, J. E., Jr. (2002) *Nat. Rev. Mol. Cell. Biol.* **3,** 651–662.
2. Decker, T. & Kovarik, P. (2000) *Oncogene* **19,** 2628–2637.
3. Wen, Z., Zhong, Z. & Darnell, J. E., Jr. (1995) *Cell* **82,** 241–250.
4. Abe, K., Hirai, M., Mizuno, K., Higashi, N., Sekimoto, T., Miki, T., Hirano, T. & Nakajima, K. (2001) *Oncogene* **20,** 3464–3474.
5. Pesu, M., Takaluoma, K., Aittomaki, S., Lagerstedt, A., Saksela, K., Kovanen, P. E. & Silvennoinen, O. (2000) *Blood* **95,** 494–502.
6. Boulton, T. G., Zhong, Z., Wen, Z., Darnell, J. E., Jr., Stahl, N. & Yancopoulos, G. D. (1995) *Proc. Natl. Acad. Sci. USA* **92,** 6915–6919.
7. Hirano, T., Ishihara, K. & Hibi, M. (2000) *Oncogene* **19,** 2548–2556.
8. Nakajima, K. & Wall, R. (1991) *Mol. Cell. Biol.* **11,** 1409–1418.
9. Nakajima, K., Kusafuka, T., Takeda, T., Fujitani, Y., Nakae, K. & Hirano, T. (1993) *Mol. Cell. Biol.* **13,** 3027–3041.
10. Ichiba, M., Nakajima, K., Yamanaka, Y., Kiuchi, N. & Hirano, T. (1998) *J. Biol. Chem.* **273,** 6132–6138.
11. Kiuchi, N., Nakajima, K., Ichiba, M., Fukada, T., Narimatsu, M., Mizuno, K., Hibi, M. & Hirano, T. (1999) *J. Exp. Med.* **189,** 63–73.
12. Yang, E., Lerner, L., Besser, D. & Darnell, J. E., Jr. (2003) *J. Biol. Chem.* **278,** 15794–15799.
13. Higashi, N., Kunimoto, H., Kaneko, S., Sasaki, T., Ishii, M., Kojima, H. & Nakajima, K. (2004) *Genes Cells* **9,** 233–242.
14. Zhao, H., Nakajima, R., Kunimoto, H., Sasaki, T., Kojima, H. & Nakajima, K. (2004) *Biochem. Biophys. Res. Commun.* **325,** 541–548.
15. Stahl, N., Farruggella, T. J., Boulton, T. G., Zhong, Z., Darnell, J. E., Jr. & Yancopoulos, G. D. (1995) *Science* **267,** 1349–1353.
16. Yamaguchi, K., Shirakabe, K., Shibuya, H., Irie, K., Oishi, I., Ueno, N., Taniguchi, T., Nishida, E. & Matsumoto, K. (1995) *Science* **270,** 2008–2011.
17. Shibuya, H., Yamaguchi, K., Shirakabe, K., Tonegawa, A., Gotoh, Y., Ueno, N., Irie, K., Nishida, E. & Matsumoto, K. (1996) *Science* **272,** 1179–1182.
18. Ninomiya-Tsuji, J., Kishimoto, K., Hiyama, A., Inoue, J., Cao, Z. & Matsumoto, K. (1999) *Nature* **398,** 252–256.
19. Irie, T., Muta, T. & Takeshige, K. (2000) *FEBS Letters* **467,** 160–164.
20. Takaesu, G., Kishida, S., Hiyama, A., Yamaguchi, K., Shibuya, H., Irie, K., Ninomiya-Tsuji, J. & Matsumoto, K. (2000) *Mol. Cell* **5,** 649–658.
21. Munoz-Sanjuan, I., Bell, E., Altmann, C. R., Vonica, A. & Brivanlou, A. H. (2002) *Development (Cambridge, U.K.)* **129,** 5529–5540.
22. Ishitani, T., Takaesu, G., Ninomiya-Tsuji, J., Shibuya, H., Gaynor, R. B. & Matsumoto, K. (2003) *EMBO J.* **22,** 6277–6288.
23. Jin, G., Klika, A., Callahan, M., Faga, B., Danzig, J., Jiang, Z., Li, X., Stark, G. R., Harrington, J. & Sherf, B. (2004) *Proc. Natl. Acad. Sci. USA* **101,** 2028–2033.
24. Moriguchi, T., Kuroyanagi, N., Yamaguchi, K., Gotoh, Y., Irie, K., Kano, T., Shirakabe, K., Muro, Y., Shibuya, H., Matsumoto, K., *et al.* (1996) *J. Biol. Chem.* **271,** 13675–13679.
25. Shirakabe, K., Yamaguchi, K., Shibuya, H., Irie, K., Matsuda, S., Moriguchi, T., Gotoh, Y., Matsumoto, K. & Nishida, E. (1997) *J. Biol. Chem.* **272,** 8141–8144.
26. Ishitani, T., Ninomiya-Tsuji, J., Nagai, S., Nishita, M., Meneghini, M., Barker, N., Waterman, M., Bowerman, B., Clevers, H., Shibuya, H., *et al.* (1999) *Nature* **399,** 798–802.
27. Ishitani, T., Kishida, S., Hyodo-Miura, J., Ueno, N., Yasuda, J., Waterman, M., Shibuya, H., Moon, R. T., Ninomiya-Tsuji, J. & Matsumoto, K. (2003) *Mol. Cell. Biol.* **23,** 131–139.
28. Kanei-Ishii, C., Ninomiya-Tsuji, J., Tanikawa, J., Nomura, T., Ishitani, T., Kishida, S., Kokura, K., Kurahashi, T., Ichikawa-Iwata, E., Kim, Y., *et al.* (2004) *Genes Dev.* **18,** 816–829.
29. Ohkawara, B., Shirakabe, K., Hyodo-Miura, J., Matsuo, R., Ueno, N., Matsumoto, K. & Shibuya, H. (2004) *Genes Dev.* **18,** 381–386.
30. Kojima, H., Nakajima, K. & Hirano, T. (1996) *Oncogene* **12,** 547–554.
31. Nakajima, K., Yamanaka, Y., Nakae, K., Kojima, H., Ichiba, M., Kiuchi, N., Kitaoka, T., Fukada, T., Hibi, M. & Hirano, T. (1996) *EMBO J.* **15,** 3651–3658.
32. Seraphin, B. (2002) *Adv. Protein. Chem.* **61,** 99–117.
33. Natsume, T., Yamauchi, Y., Nakayama, H., Shinkawa, T., Yanagida, M., Takahashi, N. & Isobe, T. (2002) *Anal. Chem.* **74,** 4725–4733.
34. Miyagishi, M. & Taira, K. (2002) *Nat. Biotech.* **20,** 497–500.
35. Miyoshi, H., Blomer, U., Takahashi, M., Gage, F. H. & Verma, I. M. (1998) *J. Virol.* **72,** 8150–8157.
36. Katayama, K., Wada, K., Miyoshi, H., Ohashi, K., Tachibana, M., Furuki, R., Mizuguchi, H., Hayakawa, T., Nakajima, A., Kadowaki, T., *et al.* (2004) *FEBS Lett.* **560,** 178–182.
37. Brott, B. K., Pinsky, B. A. & Erikson, R. L. (1998) *Proc. Natl. Acad. Sci. USA* **95,** 963–968.

Available online at www.sciencedirect.com
SCIENCE DIRECT®
DNA Repair 4 (2005) 537–545
DNA REPAIR
www.elsevier.com/locate/dnarepair

DDB2, the xeroderma pigmentosum group E gene product, is directly ubiquitylated by Cullin 4A-based ubiquitin ligase complex

Noriyuki Matsuda[a], Keiko Azuma[a,b], Masafumi Saijo[c], Shun-ichiro Iemura[d], Yusaku Hioki[d], Tohru Natsume[d], Tomoki Chiba[a], Kiyoji Tanaka[c], Keiji Tanaka[a,*]

[a] *Department of Molecular Oncology, Tokyo Metropolitan Institute of Medical Science, 3-18-22 Honkomagome, Bunkyo-ku, Tokyo 113-8613, Japan*
[b] *Department of Biology, Ochanomizu University, 2-1-1 Ohtsuka, Tokyo 112-8610, Japan*
[c] *Graduate School of Frontier Biosciences, Osaka University and Core Research for Evolutional Science and Technology (CREST), Japan Science and Technology Corporation, 1-3 Yamada-oka, Suita, Osaka 565-0871, Japan*
[d] *National Institutes of Advanced Industrial Science and Technology, Biological Information Research Center (JBIRC), Kohtoh-ku, Tokyo 135-0064, Japan*

Accepted 17 December 2004

Abstract

Xeroderma pigmentosum (XP) is a genetic disease characterized by hypersensitivity to UV irradiation and high incidence of skin cancer caused by inherited defects in DNA repair. Mutational malfunction of damaged-DNA binding protein 2 (DDB2) causes the XP complementation group E (XP-E). DDB2 together with DDB1 comprises a heterodimer called DDB complex, which is involved in damaged-DNA binding and nucleotide excision repair. Interestingly, by screening for a cellular protein(s) that interacts with Cullin 4A (Cul4A), a key component of the ubiquitin ligase complex, we identified DDB1. Immunoprecipitation confirmed that Cul4A interacts with DDB1 and also associates with DDB2. To date, it has been reported that DDB2 is rapidly degraded after UV irradiation and that overproduction of Cul4A stimulates the ubiquitylation of DDB2 in the cells. However, as biochemical analysis using pure Cul4A-containing E3 is missing, it is still unknown whether the Cul4A complex directly ubiquitylates DDB2 or not. We thus purified the Cul4A-containing E3 complex to near homogeneity and attempted to ubiquitylate DDB2 in vitro. The ubiquitylation of DDB2 was reconstituted using this pure E3 complex, indicating that DDB–Cul4A E3 complex in itself can ubiquitylate DDB2 directly. We also showed that an amino acid substitution, K244E, in DDB2 derived from a XP-E patient did not affect its ubiquitylation.

Keywords: Nucleotide excision repair; E3; Ubiquitin; DDB1; DDB2; Cullin 4A

1. Introduction

Several proteins that bind specifically to ultraviolet (UV) irradiation damaged-DNA have been discovered by electrophoretic mobility shift assay or filter-binding assay since 1970s [1]. Previous studies that have characterized the damaged-DNA binding (DDB) protein indicated that the minimal DDB complex is a heterodimer comprised of a 127 kDa DDB1 subunit and 48 kDa DDB2 subunit. The binding activity of damaged DNA is thought to reside in this heterodimeric complex (for reviews, see [2,3]).

Xeroderma pigmentosum (XP) is a rare genetic disease characterized by clinical and cellular hypersensitivity to UV radiation and high incidence of skin cancer [4]. Cells from XP patients show defective repair of DNA damage that had been induced by UV or chemical agents, and tendency for skin carcinogenesis. In 1988, Chu and Chang [5] reported that cells from XP complementation group E (XP-E) individuals (GM02415/XP2RO) lacked this damaged-DNA binding activity, suggesting that DDB is functionally involved in the XP-E disease. This is also true for some other alleles of XP-E

* Corresponding author. Tel.: +81 3 3823 2237; fax: +81 3 3823 2237.
E-mail address: tanakak@rinshoken.or.jp (K. Tanaka).

1568-7864/$ – see front matter © 2005 Elsevier B.V. All rights reserved.
doi:10.1016/j.dnarep.2004.12.012

patients [6]. Further evidence for the involvement came from microinjection experiments indicating that the purified DDB complex complements the XP-E cells' defect [7,8]. Other studies demonstrated that ectopic expression of human *DDB2* enhanced DNA repair in Chinese hamster V79 cells, which rarely express endogenous rodent *DDB2* [9]. Soon after the identification of *DDB1* and *DDB2* genes, Nichols et al. [10] revealed that *DDB2* was in fact mutated in XP-E cells lacking DDB activity. However, the molecular basis of the XP-E phenotype was ambiguous, because several groups found that cells from other patients with XP-E had normal levels of DDB activity (DDB+) and possessed no mutation in *DDB2* gene (reviewed in [2,3]). This discrepancy was puzzling until recently. Based on a thorough analysis, however, it was found that some DDB+ cell lines were mistakenly assigned to XP-E, and now it appears that all known authentic cases of XP-E are caused by *DDB2* mutations [11,12].

In eukaryotic cells, selective protein degradation is largely mediated by the ubiquitin/proteasome system. When ubiquitin is attached to the target protein by the ubiquitylation machineries, the proteasome recognizes the poly-ubiquitylated substrate to be degraded. This ubiquitin conjugating system requires the cascade reaction of three enzymes, namely E1, a ubiquitin-activating enzyme, E2, a ubiquitin-conjugating enzyme, and E3, a ubiquitin ligase. In 1999, Shiyanov et al. [13] reported that Cullin 4A (Cul4A) associates with the DDB complex. The cullin family of proteins compose a multimeric E3 complex. Cullin 1, which is the most well characterized cullin, serves as a rigid scaffold of its E3 complex and catalyses ubiquitylation through appropriate positioning of E2 and the substrate [14]. Other cullin family proteins including Cul4A are believed to function as well. The interaction between Cul4A and DDB1 was also demonstrated by several other groups recently ([15–20] and this work). These results, together with the rapid degradation of DDB2 after UV irradiation [21,22], suggest the involvement of Cullin 4A in DDB2 ubiquitylation and degradation. Strikingly, over-production of Cul4A stimulates the ubiquitylation of DDB2 [15,16]. However, since the latter studies did not show biochemical evidence of Cul4A involvement in the ubiquitylation of DDB2, it is still unknown whether the Cul4A-containing E3 complex in itself directly ubiquitylates DDB2 or not. To further investigate the mode of this ubiquitylation, an in vitro reconstitution by biochemical approach is obviously required. Here, we show that DDB2 can be ubiquitylated directly by the purified DDB–Cul4A E3 complex in a reconstitution in vitro experiment.

2. Materials and methods

2.1. Protein identification by LC–MS/MS analysis

The Cullin 4A-associated complexes were digested with *Achromobacter* protease-I and the resulting peptides were analyzed using a nanoscale LC–MS/MS system as described previously [23,24]. The peptide mixture was applied to a Mightysil-PR-18 (1 μm particle, Kanto Chemicals, Tokyo, Japan) frit-less column (45 mm × 0.150 mm i.d.) and separated using a 0–40% gradient of acetonitrile containing 0.1% formic acid over 30 min at a flow rate of 50 nl/min. Eluted peptides were sprayed directly into a quadruple time-of-flight hybrid mass spectrometer (Q-T of *Ultima*, Micromass, Manchester, UK). MS and MS/MS spectra were obtained in data-dependent mode. Up to four precursor ions above an intensity threshold of 10 counts/s were selected for MSMS analyses from each survey scan. All MS/MS spectra were searched for protein sequences of Swiss Prot and RefSeq (NCBI) using batch processes of Mascot software package (Matrix Science, London, UK).

2.2. Cell culture condition

High-Five insect cells were maintained as an adherent culture in Grace insect media (Invitrogen, Carlsbad, CA, USA) supplemented with 8% fetal bovine serum (Sigma, St. Louis, MO, USA) and 1% penicillin-streptomycin (Invitrogen). ts41 cells established from Chinese hamster [25] were maintained in Dulbecco's modified Eagle's medium (Sigma) containing 10% fetal bovine serum and 1% penicillin–streptomycin under 5% CO_2 condition at 34 °C.

2.3. Immunoprecipitation experiment

To express DDB1, DDB2 and cullin family proteins, all plasmids were constructed from pcDNA3 or pcDNA3.1 plasmid (Invitrogen). Additional details of the plasmid construction processes will be provided upon request. Mammalian ts41 cells at 48 h after DNA transfection were harvested, washed by phosphate-buffer saline (PBS) and lysed with buffer A containing 20 mM Tris–HCl, pH 7.5, 150 mM NaCl, 0.5% Nonidet P-40 and 10% glycerol. After removal of the debris by centrifugation, anti-Flag antibody (M2)-conjugated agarose (Sigma) was added to the lysate and the mixture was incubated at 4 °C for 2 h under constant rotation. After extensive washing of immunoprecipitates with buffer A, binding proteins were eluted with sodium dodecyl sulphate (SDS)-containing buffer and boiled at 95 °C for 5 min. The eluate was subjected to immunoblotting using anti-Flag (M2; Sigma), anti-Myc (Santa Cruz, Delaware, CA, USA), anti-Cul4A (our laboratory collection) and anti-DDB1 antibodies (Zymed, San Francisco, CA, USA).

2.4. Protein purification

To overproduce His-DDB1, Flag-DDB2, Cullin 4A-HA and T7-Rbx1 proteins in insect cells, the tagged full-length cDNAs were inserted into pFastBac donor plasmid (Invitrogen). Additional details of the plasmid construction processes can be provided upon request. Subsequent production of baculovirus particles was carried out according to the protocol provided by the manufacturer. Baculovirus particles for His-

DDB1 and Flag-DDB2 were used to simultaneously infect High-Five cells, as well as viruses for Cullin4A-HA and T7-Rbx1. Insect cells were incubated for 48 h after infection, washed using PBS at 4 °C and then harvested by centrifugation. The cell extract was collected using buffer B containing 20 mM Tris–HCl, pH 7.5, 0.5% Nonidet P-40, 150 mM NaCl, 100 μM $ZnSO_4$, 10 mM 2-mercaptoethanol, 6% glycerol and a protease inhibitor mixture without ethylenediaminetetraacetic acid (EDTA) (Roche, Mannheim, Germany). After centrifugation, the cell lysates were mixed together and incubated at 4 °C for 5 h with occasional gentle mixing. For initial purification, the cell lysate was loaded on a single-stranded DNA cellulose (Sigma) column equilibrated with buffer B. The column was then washed with buffer B containing 0.3 M NaCl followed by elution with buffer B containing 0.7 M NaCl. The eluted fraction was subsequently purified with nickel-chelating agarose (Qiagen, Stanford, CA, USA) pre-equilibrated with buffer B and eluted by 120 mM imidazole. This purified complex was further separated on a glycerol gradient sedimentation, which was carried out through a 10–40% glycerol gradient in 25 mM Tris–HCl, pH 7.5, 1 mM dithiothreitol (DTT) and 2 mM ATP for 22 h at 25,000 rpm ultracentrifugation. Fractions of 1 ml were collected from the top of the gradient and subjected to silver staining and immunoblotting.

To purify DDB2 (K244E)-containing complex, cell lysates containing His-DDB1, Flag-DDB2 (K244E), Cullin 4A-HA and T7-Rbx1 proteins in buffer B were collected as mentioned above. The DDB2 (K244E) complex was roughly purified with nickel-chelating agarose (Qiagen) pre-equilibrated with buffer B and eluted by 100 mM imidazole. Obtained fractions were then loaded onto HiTrap Heparin HP column (Amersham Biosciences, Piscataway, NJ, USA), washed with buffer C [20 mM Tris–HCl, pH 7.5, 150 mM NaCl, 100 μM $ZnSO_4$, 1 mM DTT, 4.5% glycerol and protease inhibitor mixture without EDTA (Roche)], and eluted with a 0.15–0.75 M NaCl gradient in buffer C. The DDB2 (K244E)-containing complex was eluted around 0.5 M NaCl and was subjected to dialysis with buffer D containing 20 mM Tris-HCl, pH 8.0, 20 mM NaCl, 100 μM $ZnSO_4$, and 1 mM DTT. A protein complex containing wild-type DDB2 was simultaneously isolated by the same method and used as a control.

To collect the authentic DDB–Cul4A complex from mammalian cells, HeLa cells stably expressing N-terminally FLAG-HA-tagged DDB2 were used. The genuine DDB–Cul4A complex was immunoprecipitated with anti-FLAG antibody followed by anti-HA antibody as described previously [17]. The eluates were further purified by Mini Q (Amersham Biosciences) column chromatography instead of glycerol density gradient centrifugation.

2.5. *In vitro ubiquitylation assay*

The ubiquitylation assay was essentially performed as described previously [26,27]. Briefly, the purified DDB–Cul4A complex was incubated in 25 mM Tris–HCl, pH 7.5, 1 mM DTT, 25 μM MG132 (Peptide Inc., Osaka, Japan), 5 mM $MgCl_2$, 100 μM $ZnSO_4$, 2 mM ATP, 50 μg of ubiquitin (Sigma)/ml, 2 μg of E1/ml and 70 μg of various E2-expressing *Escherichia coli* lysate/ml at 32 °C for 2 h and subjected to immunoblotting with anti-His (penta-His antibody; Qiagen, Stanford, CA, USA), anti-HA (HA.11, Berkeley Antibody Company, Berkeley, CA, USA), anti-Flag (M2; Sigma) and anti-T7 (Novagen, Madison, WI, USA) antibodies. In some cases, GST-ubiquitin was used instead of native ubiquitin.

3. Results

3.1. *DDB complex physically interacts with Cullin 4A*

To explore the molecular function of Cullin 4A, we examined the cellular partner(s) that interact with Cul4A in cells. A thorough analysis of human EST and genome sequences showed that the registered human Cul4A sequence (659 amino acid protein [28]) lacks its N-terminal 100 amino acid residues and thus the full-length Cul4A was obtained by PCR-assisted cDNA cloning and used hereafter. The complete nucleotide sequence of full-length Cul4A has been registered under accession number AB178950.

Flag-tagged Cul4A was expressed in HEK293 cells followed by immunoprecipitation by anti-Flag antibody. The immunoprecipitates were eluted with a Flag peptide and then digested with Lys-C endopeptides (A. protease I) and the cleaved fragments were directly analyzed using a highly sensitive "direct nano-flow LC–MS/MS" system (for detail, see Section 2). Following database search, a dozen of peptides were assigned to MS/MS spectra obtained from four nano-LC–MS/MS analyses for the Flag-Cul4A-associated complexes and DDB1 was identified as one of the Cul4A-interacting proteins.

To confirm the interaction between Cul4A and DDB1, we performed immunoprecipitation experiment. Plasmids carrying Flag-tagged cullin family proteins (Cul1, 2, 3, 4A, 4B and 5) and myc-tagged DDB1 were concurrently transfected into ts41 cells. Extracts of the transfected or mock-transfected cells were subjected to immunoprecipitation using anti-Flag antibody followed by immunoblotting with anti-DDB1 antibody. As shown in Fig. 1A, Cul4A significantly interacted with DDB1. Cul1 also bound DDB1 weakly, whereas the other Cullins tested did not interact with DDB1. We next examined whether DDB2 also associates with Cul4A, because DDB1 and DDB2 are part of the DDB complex. Plasmids carrying 6myc-tagged cullin family proteins were transfected into ts41 cells along with a plasmid harboring Flag-tagged DDB2. Each extract was then subjected to immunoprecipitation using anti-Flag antibody and immunoblotting with anti-myc antibody. Consistent with the above results, DDB2 also interacted strongly with Cul4A and weakly with Cul1 and Cul4B (Fig. 1B). DDB2 did not bind with other cullin fam-

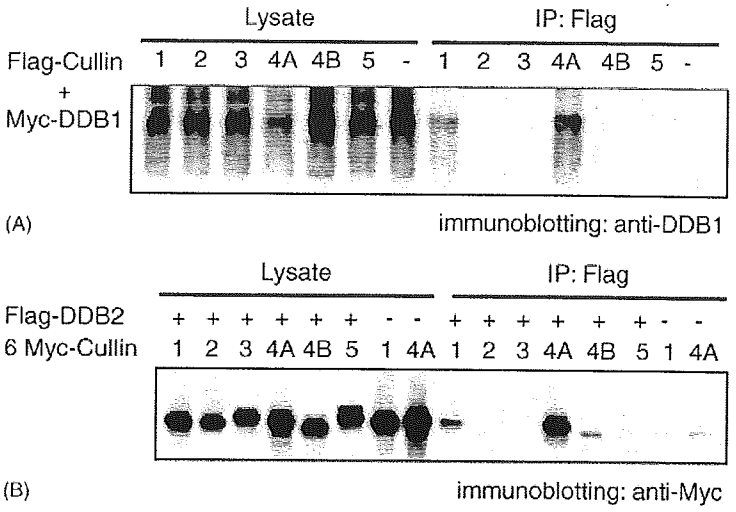

Fig. 1. DDB complex interacts with Cullin 4A. (A) Cul4A interacts with DDB1. Flag-tagged cullin family proteins and Myc-tagged DDB1 were simultaneously transfected into ts41 cells. After immunoprecipitation (IP) by anti-Flag antibody, the resulting immunoprecipitates were subjected to immunoblotting using anti-DDB1 antibody. (B) Cul4A also associates with DDB2. IP was similarly performed using FLAG-tagged DDB2 and Myc-tagged cullin family protein concurrently transfected into ts41 cells. After IP by anti-FLAG antibody, the resulting immunoprecipitates were analyzed using anti-Myc antibody.

ily proteins (Cul2, 3 and 5) examined. These results showed that DDB complex preferentially interacts with Cul4A, as reported previously [16].

3.2. Purification of DDB–Cul4A complex

We next attempted to purify DDB–Cul4A E3 complex using baculovirus expression system to perform biochemical experiments. Flag tag was fused to DDB2 at its N-terminus to facilitate its detection. This Flag-tagged DDB2 is thought to be functional because recent studies showed that ectopic expression of Flag-DDB2 enhanced DNA repair in Chinese hamster V79 cells [9], and purified Flag-DDB2 protein could restore damaged-DNA binding activity in extracts of XP-E patient cells [12]. DDB complex has been purified previously using DNA affinity column [13] and we also used DNA cellulose for initial purification of this complex. His6-tagged DDB1 and Flag-tagged DDB2 were simultaneously expressed in High-Five insect cells by the baculovirus induction system. Cul4A-HA and T7-Rbx1 were expressed concurrently as well. Each cell lysate was mixed and the resulting protein complex was purified by sequential column chromatography on single-stranded DNA cellulose, nickel-chelating agarose and subsequent 10–40% glycerol gradient by ultracentrifugation. The E3 complex comprised of DDB1, DDB2, Cul4A and Rbx1 was collected to near homogeneity as a peak fraction of glycerol gradient as shown in Fig. 2. Note that several other proteins were also detected in the final preparation (for example, a typical protein is shown by an asterisk in Fig. 2). However, since the peak fraction of such protein was inconsistent with that of the E3 complex in the glycerol gradient (data not shown), we think the protein is a contaminant derived from insect cells or a degradation product of the expressed protein, rather than a protein physiologically associated with the E3 complex.

3.3. DDB2 is ubiquitylated by purified Cul4A complex

Using this purified complex, we next tried to reconstitute the ubiquitylation of DDB2 to check whether DDB–Cul4A complex per se can ubiquitylate DDB2. Since E3 generally requires specific E2 to mediate ubiquitylation, we tested eight different E2 enzymes (E2-20k, E2-25k, Ubc3, Ubc4, UbcH5a, UbcH5c, Ubc7 and Ubc8). Slower-migrating ladders derived from auto-ubiquitylation of Cul4A (see below) were observed only from the reaction with Ubc4, UbcH5a and UbcH5c, whereas the other E2 enzymes tested did not support this modification (Fig. 3A). We thus used UbcH5 family as a source of E2 in the following experiments. Purified DDB–Cul4A complex was incubated with ATP, ubiquitin, E1 and UbcH5a, and subjected to immunoblotting with the antibody for each component. As expected, ladders derived from the auto-ubiquitylation of Cul4A were observed (Fig. 3B, single asterisk in the middle panel). Moreover, apparent high molecular-mass ladders were evident when DDB2 was detected using the anti-Flag antibody (Fig. 3B, single asterisk in the left panel). In order to demonstrate that this modification was due to ubiquitylation, we repeated the ubiquitylation assay in the presence or absence of ubiquitin. The slower migrating ladders were not detected without ubiquitin, and the addition of GST-ubiquitin instead of native ubiquitin resulted in the appearance of larger molecular-mass bands (Fig. 3B, double asterisks), indicating that this modification indeed is ubiquitylation. In the case of DDB1, a single high-molecular band also emerged after in vitro ubiquitylation (Fig. 3B, right panel). However, this ubiquitylation sig-

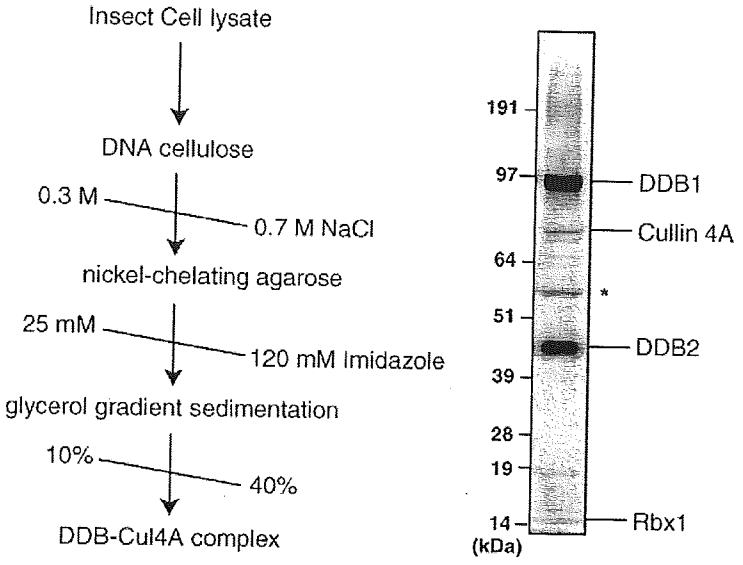

Fig. 2. Purification of the baculovirus-expressed DDB–Cul4A complex. The DDB–Cul4A complex was purified by sequential column chromatography and subsequently separated onto a 10–40% glycerol gradient by ultracentrifugation. The peak fraction of DDB–Cul4A complex was resolved by SDS-PAGE and visualized by silver staining. Asterisk shows the contaminant protein (see Section 3).

nal of DDB1 was fainter than that of Cul4A and DDB2 (see Section 4).

To further investigate the biochemical characteristics of DDB–Cul4A complex, we next purified it under more physiological conditions. HeLa cells stably expressing FLAG-HA-tagged DDB2 [17] were used to collect E3 complex. The DDB2-containing complex was immunoprecipitated with anti-FLAG antibody followed by anti-HA antibody as described previously [17] and the eluates were further purified by Mini Q column chromatography. The authentic E3 complex, comprised of DDB1, DDB2, Cul4A and Rbx1, was purified to almost homogeneity (Fig. 4A). When this complex was incubated with ATP, ubiquitin, E1 and UbcH5a, apparent high molecular-mass ladders derived from the ubiquity-

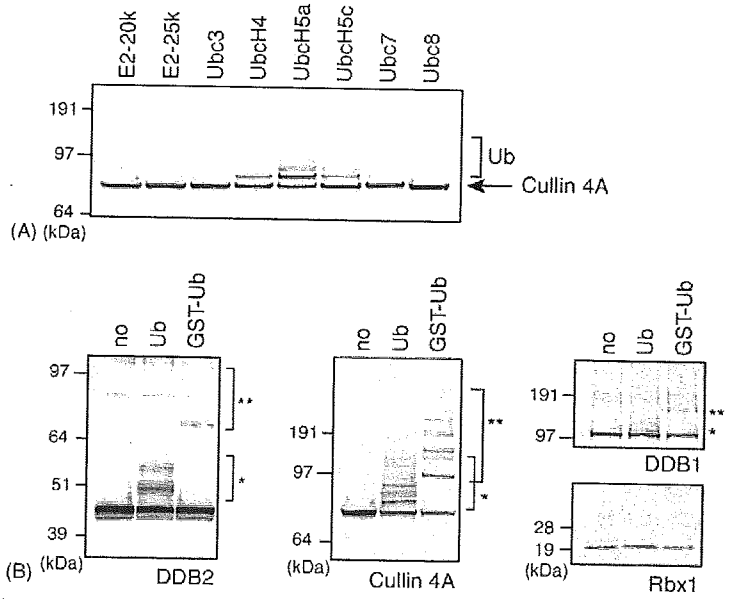

Fig. 3. In vitro reconstitution of DDB2 ubiquitylation. (A) The DDB–Cul4A E3 complex cooperates with Ubc4 and UbcH5 subfamily of E2 enzymes. Purified DDB–Cul4A E3 was incubated with the indicated E2 enzymes and subjected to immunoblotting with anti-HA antibody to identify the auto-ubiquitylation. (B) DDB2 was directly ubiquitylated by the DDB–Cul4A complex. Pure DDB1–DDB2-Cul4A complex was subjected to in vitro ubiquitylation assay in the absence (no) or presence of ubiquitin (Ub) or GST-ubiquitin (GST-Ub) and analyzed by immunoblotting with each antibody. Single asterisks show the ubiquitin conjugation and double asterisks indicate GST-ubiquitin conjugation.

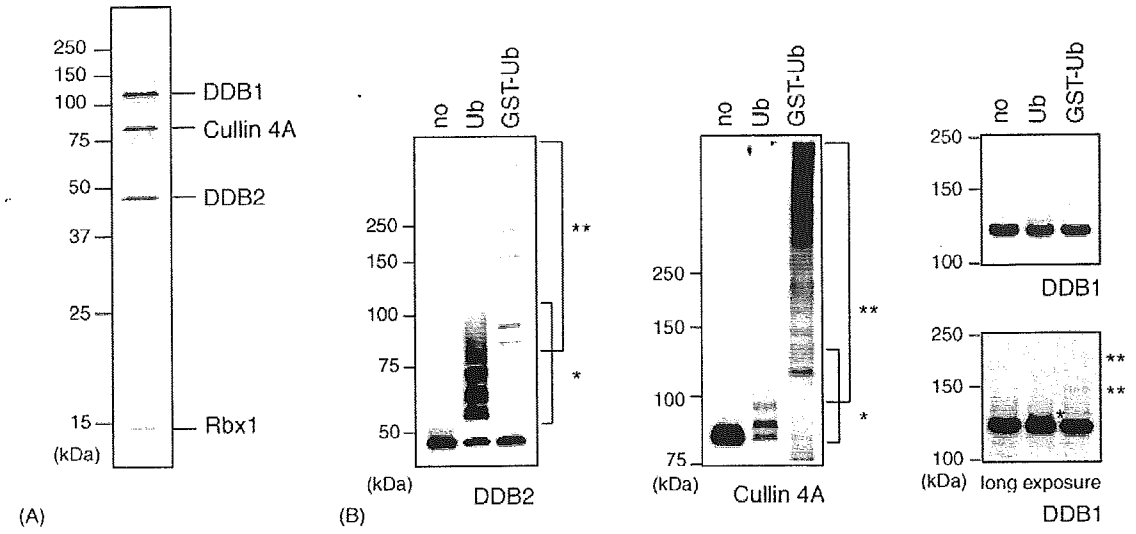

Fig. 4. In vitro ubiquitylation of DDB2 using authentic DDB–Cul4A complex. (A) Purification of the genuine DDB–Cul4A complex. Purified complex was resolved by SDS-PAGE and visualized by silver staining. (B) In vitro ubiquitylation of DDB2 and auto-ubiquitylation of Cul4A. The authentic DDB–Cul4A complex was subjected to in vitro ubiquitylation assay in the absence (no) or presence of ubiquitin (Ub) or GST-ubiquitin (GST-Ub) and analyzed by immunoblotting with anti-HA (DDB2), anti-Cul4A and anti-DDB1 antibodies. Single asterisks show the ubiquitin conjugation and double asterisks indicate GST-ubiquitin conjugation.

lation of DDB2 and Cul4A were again observed (Fig. 4B, single asterisk). The exclusion of ubiquitin from the assay quenched these bands and replacement of native ubiquitin with GST-ubiquitin retarded their mobility (Fig. 4B, double asterisks). In contrast, DDB1 was rarely ubiquitylated, although a faint ubiquitylation signal was observed after long exposure (Fig. 4B, right panel). Because the DDB–Cul4A complex derived from both insect (Fig. 3) and mammalian (Fig. 4) cells directly ubiquitylated DDB2, we concluded that DDB2 was ubiquitylated by genuine DDB–Cul4A complex.

3.4. XP-E mutation does not affect ubiquitylation of DDB2 in vitro

Two cell lines established from XP-E patients, XP2RO and XP82TO, have been characterized in detail. XP2RO and XP82TO cells harbor naturally occurring single amino acid substitutions, R273H and K244E, in DDB2 protein, respectively. It has been reported that the XP82TO mutant protein (DDB2-K244E) interacts normally with DDB1 and Cullin 4A. Conversely, XP2RO mutant protein (DDB2-R273H) interacts with neither of them [13,29]. We also confirmed by immunoprecipitation experiments that DDB2-K244E interacts with DDB1 and Cullin 4A normally, but DDB2-R273H did not associate with either of them (Fig. 5A). Intriguingly, Rapic-Otrin et al. [21] reported that UV-induced rapid degradation of DDB2 protein did not occur in XP82TO cell line. This information prompted us to test whether K244E mutation affects the in vitro ubiquitylation of DDB2. Because DDB1–DDB2 (K244E)-Cul4A complex did not interact effectively with DNA cellulose, we were unable to purify it compared with the wild-type complex (data not shown). We thus purified this mutant protein complex by affinity chromatography on nickel-chelating column and subsequent heparin column, and the bound DDB2 (K244E) complex was eluted around 0.5 M NaCl (Fig. 5B). As a control, the wild type DDB2-containing complex was simultaneously isolated by the same method. The DDB1–DDB2 (K244E)-Cul4A complex was incubated with ATP, ubiquitin, E1 and UbcH5a, and subjected to immunoblotting with the anti-Flag antibody. The mutant DDB2 protein was ubiquitylated in a manner equivalent to that of the wild-type control (Fig. 5C), indicating that XP82TO mutation (K244E) did not affect the ubiquitylation of DDB2 in vitro. This result also suggests that the mutated site of DDB2 (244th K) per se is not the unique ubiquitylation site.

4. Discussion

The DDB complex is regulated through several processes when cells are exposed to UV irradiation, namely very rapid translocation into the nucleus and binding to chromatin [17,29–31], hasty degradation of DDB2 protein [21,22] and final transcriptional induction of *DDB2* mRNA [32,33]. Chemical inhibition of proteasomes prevents rapid degradation of DDB2 protein, suggesting that this process is mediated by the ubiquitin/proteasome system. Among these regulation processes of DDB2, proteolytic degradation is the most intriguing because several recent reports [13,15–17] and our present results have shown a tight relationship between the DDB complex and proteins involved in ubiquitylation.

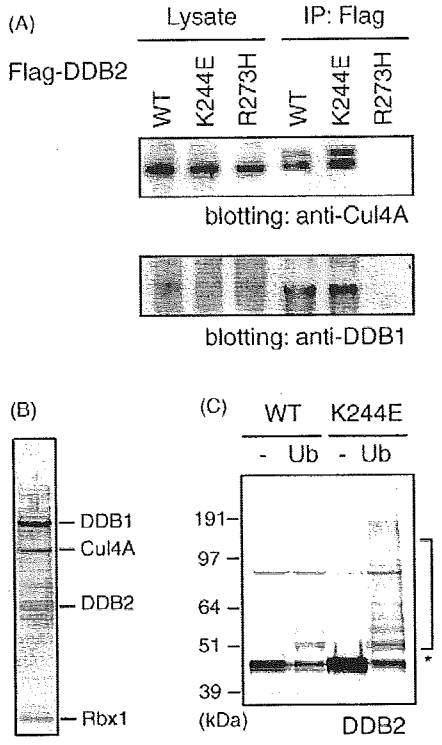

Fig. 5. XP82TO mutation (K244E) does not affect the in vitro ubiquitylation of DDB2. (A) DDB2-K244E interacts with DDB1 and Cul4A, but DDB2-R273H associates with neither. Flag-DDB2 (WT, K244E or R273H) was co-transfected with Myc-Cul4A and HA-DDB1 into ts41 cells. After immunoprecipitation (IP) by anti-Flag antibody, the resulting immunoprecipitates were subjected to immunoblotting using anti-Cul4A and anti-DDB1 antibodies. (B) The DDB2 (K244E) complex was resolved by SDS-PAGE and visualized by silver staining. (C) Ubiquitylation of DDB2 protein with XP-E mutation (DDB2-K244E) was comparable with that of wild-type DDB2 in vitro. The DDB–Cul4A complex containing mutant or wild type DDB2 was subjected to in vitro ubiquitylation in the presence (Ub) or absence (-) of ubiquitin. Asterisk indicates the ubiquitin-conjugated DDB2.

Interestingly, ectopic over-production of Cullin 4A accelerates the degradation of DDB2, suggesting that Cul4A ubiquitylates DDB2 [15,16]. However, no reconstitution experiments were performed and thus this information did not exclude the possible involvement of other E3(s) downstream of Cul4A in the ubiquitylation of DDB2, rather than directly by Cul4A. This situation prompted us to reconstitute the in vitro ubiquitylation of DDB2 and we presented in this study biochemical evidence for the ubiquitylation of DDB2 directly by the DDB–Cullin 4A complex.

4.1. In vitro ubiquitylation of each subunit of the DDB complex

It is well established that a significant fraction of DDB2 is degraded promptly after UV irradiation [21,22] and is also degraded in a cell cycle-dependent manner [16]. Conversely, it is still controversial whether another component of the DDB complex, DDB1, is a target of ubiquitylation and subsequent degradation. Zhou's group reported that overproduction of Cul4A in cells stimulates the ubiquitylation of DDB1 [15]. In contrast, neither ectopically expressed Cul4A nor UV irradiation accelerates degradation of DDB1 was reported by other groups [12,16]. In our reconstitution experiment, DDB1 was very weakly ubiquitylated in the DDB–Cul4A complex from insect cells (Fig. 3B) and seldom ubiquitylated in the complex from HeLa cells (Fig. 4B). Because the HeLa cell-derived complex is purer and was considered to be isolated under more physiological conditions, this result supports the notion that DDB1 is not ubiquitylated by the Cul4A E3 complex. Even though DDB1 was faintly ubiquitylated, such mono- or di-ubiquitylation is insufficient for the proteasomal degradation. Therefore, we favor the scenario that not DDB1 but DDB2 is the target of ubiquitylation by Cul4A E3 complex in vivo [12,16].

4.2. XP-E mutation did not affect the ubiquitylation of p48 in vitro

Rapic-Otrin et al. [21] reported that UV-induced rapid degradation of DDB2 did not occur in the XP-E cell line (XP82TO) whose DDB2 harbors a K244E mutation. Because this mutant protein (DDB2-K244E) can interact with DDB1 and Cullin 4A (Fig. 5A [13]) but not with damaged DNA [8,12,34], this result suggests that the binding activity to damaged-DNA is necessary for the degradation of DDB2. Another possibility is that the mutated site of DDB2 (244th K) per se is the main ubiquitylation site, as suggested previously [21]. However, the latter is unlikely because we showed that this mutant protein was still ubiquitylated in a manner similar to the wild-type DDB2 protein in vitro (Fig. 5C). Perhaps binding to damaged-DNA renders the conformation of DDB complex more acquiescent for ubiquitylation and/or UV recruits DDB to some specialized chromatin place where the other ubiquitylation machinery is easy to access in vivo.

4.3. Biochemical role of DDB in nucleotide excision repair

In XP-E cells lacking the DDB activity, the nucleotide excision repair (NER) of cyclobutane pyrimidine dimer (CPD) is significantly impaired [32], suggesting the importance of DDB complex in NER in vivo. However, this DDB complex is not essential for the reconstitution of the cell-free NER in vitro. The NER reaction was successfully reconstituted in the absence of DDB [35–37], although it may exhibit some stimulatory or inhibitory effects under certain conditions [38–40]. One interpretation of these results is that some partner protein(s) of DDB complex may be missing in such NER assay in vitro. Recent studies [13,15–20,41–43] and the present work emphasize the role of the DDB1 complex in the ubiquitin ligation. We can thus speculate that the effect and requirement of DDB could change if other ubiquitylation machinery was added to the in vitro NER assay.

4.4. Biological function of DDB2 ubiquitylation

As mentioned above, DDB2 protein is rapidly degraded after UV-irradiation in vivo [21,22] and we showed here that the DDB–Cul4A complex could directly ubiquitylate DDB2. What is the function of DDB2 ubiquitylation and subsequent degradation? After damaged-DNA recognition, DDB is thought to hand over the DNA lesion to the following NER component(s) including XPC [2]. An appealing hypothesis is that clearance of DDB2 by ubiquitylation and succeeding degradation facilitates accession of the following NER factor(s) to the DNA lesion. However, it is not clear at present whether the ubiquitylation of DDB2 is only required for its UV-induced degradation, or is essential to change some biological character of DDB2 preceding degradation. Because various non-proteolytic functions of ubiquitylation have been identified recently [44], it is still conceivable that the ubiquitylation of DDB2 might have an additional role besides degradation. Moreover, we still do not know whether DDB2 ubiquitylation is a pertinent event for DDB function in DNA repair, or is the only side effect accompanied by ubiquitylation of authentic, relevant substrate. To define the precise role of DDB–Cullin 4A complex-mediated ubiquitylation, further studies are obviously required; especially the identification of the physiological substrate. Such experiments are currently underway in our laboratories.

Acknowledgements

We are grateful to Dr. Yoshihiro Nakatani of Harvard Medical School for providing HeLa cells expressing epitope-tagged DDB2 and to Dr. Kaoru Sugasawa of RIKEN for the critical reading of the manuscript. We also thank all members of Prof. K. Tanaka laboratory for the helpful discussions. This work was supported by CREST of Japan Science and Technology (JST), Takeda Science Foundation (to M.S.) and Grants-in-Aid from the Ministry of Education, Culture, Sports, Science and Technology of Japan (to K.T.).

References

[1] R.S. Feldberg, L. Grossman, A DNA binding protein from human placenta specific for ultraviolet damaged DNA, Biochemistry 15 (1976) 2402–2408.
[2] J. Tang, G. Chu, Xeroderma pigmentosum complementation group E and UV-damaged DNA-binding protein, DNA Repair 1 (2002) 601–616.
[3] B.B.O. Wittschieben, R.D. Wood, DDB complexities, DNA Repair 2 (2003) 1065–1069.
[4] D. Bootsma, K.H. Kraemer, J.E. Cleaver, J.H.J. Hoeijmakers, Nucleotide excision repair syndromes: xeroderma pigmentosum, Cockayne syndrome and trichothiodystrophy, in: B. Vogelstein, K.W. Kinzler (Eds.), The Genetic Basis of Human Cancer, McGraw Hill, New York, 1997, pp. 245–274.
[5] G. Chu, E. Chang, Xeroderma pigmentosum group E cells lack a nuclear factor that binds to damaged DNA, Science 242 (1988) 564–567.
[6] B.J. Hwang, S. Toering, U. Francke, G. Chu, p48 activates a UV-damaged-DNA binding factor and is defective in xeroderma pigmentosum group E cells that lack binding activity, Mol. Cell. Biol. 18 (1998) 4391–4399.
[7] S. Keeney, A.P. Eker, T. Brody, W. Vermeulen, D. Bootsma, J.H. Hoeijmakers, S. Linn, Correction of the DNA repair defect in xeroderma pigmentosum group E by injection of a DNA damage-binding protein, Proc. Natl. Acad. Sci. U.S.A. 91 (1994) 4053–4056.
[8] V. Rapic-Otrin, I. Kuraoka, T. Nardo, M. McLenigan, A.P. Eker, M. Stefanini, A.S. Levine, R.D. Wood, Relationship of the xeroderma pigmentosum group E DNA repair defect to the chromatin and DNA binding proteins UV-DDB and replication protein A, Mol. Cell. Biol. 18 (1998) 3182–3190.
[9] J.Y. Tang, B.J. Hwang, J.M. Ford, P.C. Hanawalt, G. Chu, Xeroderma pigmentosum p48 gene enhances global genomic repair and suppresses UV-induced mutagenesis, Mol. Cells 5 (2000) 737–744.
[10] A.F. Nichols, P. Ong, S. Linn, Mutations specific to the xeroderma pigmentosum group E Ddb-phenotype, J. Biol. Chem. 271 (1996) 24317–24320.
[11] T. Itoh, S. Linn, T. Ono, M. Yamaizumi, Reinvestigation of the classification of five cell strains of xeroderma pigmentosum group E with reclassification of three of them, J. Invest. Dermatol. 114 (2000) 1022–1029.
[12] V. Rapic-Otrin, V. Navazza, T. Nardo, E. Botta, M. McLenigan, D.C. Bisi, A.S. Levine, M. Stefanini, True XP group E patients have a defective UV-damaged DNA binding protein complex and mutations in DDB2 which reveal the functional domains of its p48 product, Hum. Mol. Genet. 12 (2003) 1507–1522.
[13] P. Shiyanov, A. Nag, P. Raychaudhuri, Cullin 4A associates with the UV-damaged DNA-binding protein DDB, J. Biol. Chem. 274 (1999) 35309–35312.
[14] N. Zheng, B.A. Schulman, L. Song, J.J. Miller, P.D. Jeffrey, P. Wang, C. Chu, D.M. Koepp, S.J. Elledge, M. Pagano, R.C. Conaway, J.W. Conaway, J.W. Harper, N.P. Pavletich, Structure of the Cul1-Rbx1-Skp1-F boxSkp2 SCF ubiquitin ligase complex, Nature 416 (2002) 703–709.
[15] X. Chen, Y. Zhang, L. Douglas, P. Zhou, UV-damaged DNA-binding proteins are targets of CUL-4A-mediated ubiquitination and degradation, J. Biol. Chem. 276 (2001) 48175–48182.
[16] A. Nag, T. Bondar, S. Shiv, P. Raychaudhuri, The xeroderma pigmentosum group E gene product DDB2 is a specific target of cullin 4A in mammalian cells, Mol. Cell. Biol. 21 (2001) 6738–6747.
[17] R. Groisman, J. Polanowska, I. Kuraoka, J. Sawada, M. Saijo, R. Drapkin, A.F. Kisselev, K. Tanaka, Y. Nakatani, The ubiquitin ligase activity in the DDB2 and CSA complexes is differentially regulated by the COP9 signalosome in response to DNA damage, Cell 113 (2003) 357–367.
[18] C. Liu, K.A. Powell, K. Mundt, L. Wu, A.M. Carr, T. Caspari, Cop9/signalosome subunits and Pcu4 regulate ribonucleotide reductase by both checkpoint-dependent and -independent mechanisms, Genes Dev. 17 (2003) 1130–1140.
[19] T. Bondar, A. Ponomarev, P. Raychaudhuri, Ddb1 is required for the proteolysis of the *Schizosaccharomyces pombe* replication inhibitor Spd1 during S phase and after DNA damage, J. Biol. Chem. 279 (2004) 9937–9943.
[20] I.E. Wertz, K.M. O'Rourke, Z. Zhang, D. Dornan, D. Arnott, R.J. Deshaies, V.M. Dixit, Human De-etiolated-1 regulates c-Jun by assembling a CUL4A ubiquitin ligase, Science 303 (2004) 1371–1374.
[21] V. Rapic-Otrin, M.P. McLenigan, D.C. Bisi, M. Gonzalez, A.S. Levine, Sequential binding of UV DNA damage binding factor and degradation of the p48 subunit as early events after UV irradiation, Nucleic Acids Res. 30 (2002) 2588–2598.
[22] M.E. Fitch, I.V. Cross, S.J. Turner, S. Adimoolam, C.X. Lin, K.G. Williams, J.M. Ford, The DDB2 nucleotide excision repair gene product p48 enhances global genomic repair in p53 deficient human fibroblasts, DNA Repair 2 (2003) 819–826.

[23] T. Natsume, Y. Yamauchi, H. Nakayama, T. Shinkawa, M. Yanagida, N. Takahashi, T. Isobe, A direct nanoflow liquid chromatography-tandem mass spectrometry system for interaction proteomics, Anal. Chem. 74 (2002) 4725–4733.
[24] M. Komatsu, T. Chiba, K. Tatsumi, S.-I. Iemura, I. Tanida, N. Okazaki, T. Ueno, E. Kominami, T. Natsume, K. Tanaka, A novel protein-conjugating system for Ufm1, a ubiquitin-fold modifier, EMBO J. 23 (2004) 1977–1986.
[25] S. Handeli, H. Weintraub, The ts41 mutation in Chinese hamster cells leads to successive S phases in the absence of intervening G2, M, and G1, Cell 71 (1992) 599–611.
[26] N. Matsuda, T. Suzuki, K. Tanaka, A. Nakano, Rma1, a novel type of RING finger protein conserved from Arabidopsis to human, is a membrane-bound ubiquitin ligase, J. Cell Sci. 114 (2001) 1949–1957.
[27] N. Imai, N. Matsuda, K. Tanaka, A. Nakano, S. Matsumoto, W. Kang, Ubiquitin ligase activities of Bombyx mori nucleopolyhedrovirus RING finger proteins, J. Virol. 77 (2003) 923–930.
[28] L.C. Chen, S. Manjeshwar, Y. Lu, D. Moore, B.M. Ljung, W.L. Kuo, S.H. Dairkee, M. Wernick, C. Collins, H.S. Smith, The human homologue for the *Caenorhabditis elegans* cul-4 gene is amplified and overexpressed in primary breast cancers, Cancer Res. 58 (1998) 3677–3683.
[29] P. Shiyanov, S.A. Hayes, M. Donepudi, A.F. Nichols, S. Linn, B.L. Slagle, P. Raychaudhuri, The naturally occurring mutants of DDB are impaired in stimulating nuclear import of the p125 subunit and E2F1-activated transcription, Mol. Cell. Biol. 19 (1999) 4935–4943.
[30] V. Rapic-Otrin, M. McLenigan, M. Takao, A.S. Levine, M. Protic, Translocation of a UV-damaged DNA binding protein into a tight association with chromatin after treatment of mammalian cells with UV light, J. Cell Sci. 110 (1997) 1159–1168.
[31] W. Liu, A.F. Nichols, J.A. Graham, R. Dualan, A. Abbas, S. Linn, Nuclear transport of human DDB protein induced by ultraviolet light, J. Biol. Chem. 275 (2000) 21429–21434.
[32] B.J. Hwang, J.M. Ford, P.C. Hanawalt, G. Chu, Expression of the p48 xeroderma pigmentosum gene is p53-dependent and is involved in global genomic repair, Proc. Natl. Acad. Sci. U.S.A. 96 (1999) 424–428.
[33] T. Itoh, C. O'Shea, S. Linn, Impaired regulation of tumor suppressor p53 caused by mutations in the xeroderma pigmentosum DDB2 gene: mutual regulatory interactions between p48(DDB2) and p53, Mol. Cell. Biol. 23 (2003) 7540–7553.
[34] S. Keeney, H. Wein, S. Linn, Biochemical heterogeneity in xeroderma pigmentosum complementation group E, Mutat. Res. 273 (1992) 49–56.
[35] M. Araki, C. Masutani, T. Maekawa, Y. Watanabe, A. Yamada, R. Kusumoto, D. Sakai, K. Sugasawa, Y. Ohkuma, F. Hanaoka, Reconstitution of damage DNA excision reaction from SV40 minichromosomes with purified nucleotide excision repair proteins, Mutat. Res. 459 (2000) 147–160.
[36] S.J. Araujo, F. Tirode, F. Coin, H. Pospiech, J.E. Syvaoja, M. Stucki, U. Hubscher, J.M. Egly, R.D. Wood, Nucleotide excision repair of DNA with recombinant human proteins: definition of the minimal set of factors, active forms of TFIIH, and modulation by CAK, Genes Dev. 14 (2000) 349–359.
[37] D. Mu, C.H. Park, T. Matsunaga, D.S. Hsu, J.T. Reardon, A. Sancar, Reconstitution of human DNA repair excision nuclease in a highly defined system, J. Biol. Chem. 270 (1995) 2415–2418.
[38] A. Aboussekhra, M. Biggerstaff, M.K. Shivji, J.A. Vilpo, V. Moncollin, V.N. Podust, M. Protic, U. Hubscher, J.M. Egly, R.D. Wood, Mammalian DNA nucleotide excision repair reconstituted with purified protein components, Cell 80 (1995) 859–868.
[39] M. Wakasugi, M. Shimizu, H. Morioka, S. Linn, O. Nikaido, T. Matsunaga, Damaged DNA-binding protein DDB stimulates the excision of cyclobutane pyrimidine dimers in vitro in concert with XPA and replication protein A, J. Biol. Chem. 276 (2001) 15434–15440.
[40] M. Wakasugi, A. Kawashima, H. Morioka, S. Linn, A. Sancar, T. Mori, O. Nikaido, T. Matsunaga, DDB accumulates at DNA damage sites immediately after UV irradiation and directly stimulates nucleotide excision repair, J. Biol. Chem. 277 (2002) 1637–1640.
[41] Y. Yanagawa, J.A. Sullivan, S. Komatsu, G. Gusmaroli, G. Suzuki, J. Yin, T. Ishibashi, Y. Saijo, V. Rubio, S. Kimura, J. Wang, X.W. Deng, Arabidopsis COP10 forms a complex with DDB1 and DET1 in vivo and enhances the activity of ubiquitin conjugating enzymes, Genes Dev. 18 (2004) 2172–2181.
[42] L.A. Higa, I.S. Mihaylov, D.P. Banks, J. Zheng, H. Zhang, Radiation-mediated proteolysis of CDT1 by CUL4-ROC1 and CSN complexes constitutes a new checkpoint, Nat. Cell Biol. 5 (2003) 1008–1015.
[43] J. Hu, C.M. McCall, T. Ohta, Y. Xiong, Targeted ubiquitination of CDT1 by the DDB1–CUL4A-ROC1 ligase in response to DNA damage, Nat. Cell Biol. 6 (2004) 1003–1009.
[44] J.D. Schnell, L. Hicke, Non-traditional functions of ubiquitin and ubiquitin-binding proteins, J. Biol. Chem. 278 (2003) 35857–35860.

THE JOURNAL OF BIOLOGICAL CHEMISTRY VOL. 280, NO. 52, pp. 42685–42693, December 30, 2005

WNK1 Regulates Phosphorylation of Cation-Chloride-coupled Cotransporters via the STE20-related Kinases, SPAK and OSR1*[S]

Received for publication, September 13, 2005, and in revised form, October 27, 2005 Published, JBC Papers in Press, October 31, 2005, DOI 10.1074/jbc.M510042200

Tetsuo Moriguchi[‡§], Seiichi Urushiyama[‡], Naoki Hisamoto[¶], Shun-ichiro Iemura[‖], Shinichi Uchida[**], Tohru Natsume[‖], Kunihiro Matsumoto[¶], and Hiroshi Shibuya[‡§1]

From the [‡]Department of Molecular Cell Biology, Medical Research Institute and School of Biomedical Science, Tokyo Medical and Dental University, and CREST, JST, Chiyoda, Tokyo 101-0062, the [§]Center of Excellence Program for Frontier Research on Molecular Destruction and Reconstruction of Tooth and Bone, Kanda-Surugadai, Chiyoda, Tokyo 101-0062, the [¶]Department of Molecular Biology, Graduate School of Science, Nagoya University and CREST, JST, Chikusa-ku, Nagoya 464-8602, the [‖]National Institutes of Advanced Industrial Science and Technology, Biological Information Research Center (JBIRC), Kohtoh-ku, Tokyo 135-0064, and the [**]Department of Nephrology, Graduate School of Medicine, Tokyo Medical and Dental University, Bunkyo, Tokyo 113-8519, Japan

The WNK1 and WNK4 genes have been found to be mutated in some patients with hyperkalemia and hypertension caused by pseudohypoaldosteronism type II. The clue to the pathophysiology of pseudohypoaldosteronism type II was its striking therapeutic response to thiazide diuretics, which are known to block the sodium chloride cotransporter (NCC). Although this suggests a role for WNK1 in hypertension, the precise molecular mechanisms are largely unknown. Here we have shown that WNK1 phosphorylates and regulates the STE20-related kinases, Ste20-related proline-alanine-rich kinase (SPAK) and oxidative stress response 1 (OSR1). WNK1 was observed to phosphorylate the evolutionary conserved serine residue located outside the kinase domains of SPAK and OSR1, and mutation of the OSR1 serine residue caused enhanced OSR1 kinase activity. In addition, hypotonic stress was shown to activate SPAK and OSR1 and induce phosphorylation of the conserved OSR1 serine residue, suggesting that WNK1 may be an activator of the SPAK and OSR1 kinases. Moreover, SPAK and OSR1 were found to directly phosphorylate the N-terminal regulatory regions of cation-chloride-coupled cotransporters including NKCC1, NKCC2, and NCC. Phosphorylation of NCC was induced by hypotonic stress in cells. These results suggested that WNK1 and SPAK/OSR1 mediate the hypotonic stress signaling pathway to the transporters and may provide insights into the mechanisms by which WNK1 regulates ion balance.

WNK[2] kinases (with no lysine (K)) comprise a family of novel serine/threonine protein kinases conserved among multicellular organisms (1, 2). The kinase domain of this family is unique in that it lacks the conserved lysine residue previously known to be important for ATP binding in the catalytic site. A conserved lysine in subdomain I of the WNK kinases is thought to be essential for their catalytic activity (1, 3). There are four human WNK family members. *WNK1* and *WNK4* were identified as genes mutated in families of patients with pseudohypoaldosteronism type 2 (PHA II) human hypertension (4). The *WNK1* gene mutation consists of a deletion within its first intron, leading to increased expression, whereas mutations in the *WNK4* gene are found in the coding sequence near the coiled-coil domains.

PHA II patients are treated by thiazide diuretics, which function as antagonists of the Na-Cl cotransporter (NCC, also known as thiazide-sensitive cotransporter (TSC) or Na-Cl transporter (NCCT)), suggesting that the activity of NCC could be potentially involved in the development of PHA II. Previous studies using *Xenopus* oocytes have showed that wild-type WNK4 inhibits the surface expression and the activity of NCC, whereas one of the disease-causing mutants of WNK4 attenuated this inhibitory effect (5, 6). However, comparison of wild-type and mutant WNK4 revealed no differences in NCC surface expression in polarized epithelial cells (MDCK II cells), suggesting that the regulation of intracellular NCC localization by WNK4 might be unrelated to the pathogenesis of PHA II (7). WNK4 has also been reported to inhibit surface expression of the secretory potassium channel (ROMK) and Cl^- base exchanger SCL26A6 (CFEX), in addition to NCC, in *Xenopus* oocytes (8, 9). Furthermore, the disease-causing mutant of WNK4 was shown to increase paracellular chloride permeability in MDCK cells (10, 11). In contrast to WNK4, little is known about the functions and regulation of WNK1. WNK1 does not directly affect NCC activity in *Xenopus* oocytes but has been shown to modulate the inhibitory effects of WNK4 on NCC (6). Although WNK1 activates the MEK5-ERK5 pathway and phosphorylates synaptotagmin, there is no direct evidence to link WNK1 and transporter function (12, 13). Moreover, a recent study reported that WNK1 regulates the epithelial sodium channel through glucocorticoid-inducible kinase (SGK1), but the mechanisms of SGK1 activation by WNK1 have not been fully elucidated (14, 15).

NCC contains 12 transmembrane domains and is closely related to the Na-K-2Cl cotransporters, NKCC1 and NKCC2 (16–18). NCC and NKCC2 are expressed in the kidney and function in renal salt reabsorption, whereas NKCC1 is expressed ubiquitously and plays a key role in

* This work was supported by the Center of Excellence Program for Frontier Research on Molecular Destruction and Reconstruction of Tooth and Bone, grants-in-aid for scientific research from the Ministry of Education, Science, Sports and Culture of Japan, and grants provided by the Ichiro Kanehara Foundation, the Naito Foundation, the Yamanouchi Foundation for Research on Metabolic Disorders, and the Center of Excellence Program for Frontier Research. The costs of publication of this article were defrayed in part by the payment of page charges. This article must therefore be hereby marked "*advertisement*" in accordance with 18 U.S.C. Section 1734 solely to indicate this fact.

[S] The on-line version of this article (available at http://www.jbc.org) contains a supplemental figure showing the specificity of anti-SPAK/OSR1 and anti-OSR1-P antibodies.

[1] To whom correspondence should be addressed. Tel. and Fax: 81-3-5280-8062, E-mail: shibuya.mcb@mri.tmd.ac.jp.

[2] The abbreviations used are: WNK, with no lysine (K); NCC, Na-Cl cotransporter; KCC, K-Cl cotransporter; NKCC, Na-K-2Cl cotransporter; SPAK, Ste20-related proline-alanine-rich kinase; OSR1, oxidative stress response 1; ERK, extracellular signal-regulated kinase; MEK, mitogen-activated protein kinase/extracellular signal-regulated kinase kinase; MS, mass spectrometry; LC-MS/MS, liquid chromatography coupled to tandem MS; GST, glutathione S-transferase; PHA II, pseudohypoaldosteronism type 2; MDCK, Madin-Darby canine kidney cells.

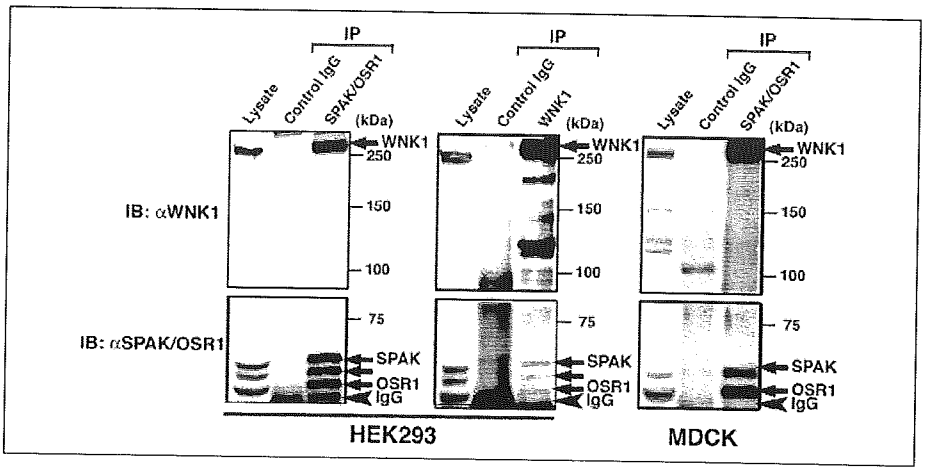

FIGURE 1. **Association of WNK1 with SPAK and OSR1.** SPAK and OSR1 were immunoprecipitated (*IP*) from 0.4 mg of lysates prepared from HEK293 cells (*left*) or MDCK cells (*right*) with 2 μg of SPAK/OSR1 antibody, fractionated by SDS-PAGE, and immunoblotted (*IB*) with the indicated antibodies. WNK1 was immunoprecipitated from 1 mg of HEK293 lysates with 10 μg of the WNK1 antibody (*middle*). As a control, immunoprecipitations were also performed in parallel experiments with rabbit IgG (Chemicon International).

epithelial salt secretion and cell volume regulation. NKCC1 cotransport activity is controlled by the phosphorylation/dephosphorylation of several threonine and serine residues in response to decreases in cell volume or intracellular [Cl]. Three of the phosphoacceptors in the N terminus of NKCC1 have been identified, and the amino acid sequences surrounding these residues are highly conserved among the members of the cation-chloride-coupled cotransporter family, suggesting that phospho-regulatory mechanisms are conserved among these cotransporters (19). Although several protein kinases, such as SGK1 and c-Jun N-terminal kinase, have been proposed as candidates for the activators of NKCC1, there is no evidence showing that any kinase directly phosphorylates NKCC1 *in vivo* (20, 21). It has been previously reported that the STE20-related kinases, SPAK (also called PASK (proline-alanine-rich Ste-20-related kinase)) and OSR1, bind to the N-terminal regions of the cation-chloride cotransporters KCC3, NKCC1, and NKCC2 (22). Moreover, WNK4 has been identified as a putative SPAK-binding protein by yeast two-hybrid screening (23). Expression of a dominant-negative form of SPAK decreased cotransport activity and phosphorylation of NKCC1 (24). Therefore, SPAK is thought to play an important role in the regulation of NKCC1.

In this study, we have identified SPAK as a WNK1-binding protein and provided evidence that WNK1 acts as a direct activator of SPAK and OSR1. Moreover, we have shown that SPAK and OSR1 directly phosphorylate the N-terminal regulatory regions of NKCC1, NKCC2, and NCC. These results have raised the possibility that WNK1 regulates the activities of a number of transporters through SPAK/OSR1 and that this regulation contributes to the pathogenesis of hypertension.

EXPERIMENTAL PROCEDURES

Molecular Cloning and Plasmid Construction—Human WNK1, human WNK4, rat SPAK, human NKCC1, human NKCC2, mouse NCC, and mouse OSR1 coding regions were amplified by PCR using Marathon-Ready cDNA (Clontech) as templates. GST-PAK3-(65–135) expression plasmid was kindly provided by T. Akiyama (25). To construct mammalian expression vectors, pCMV-FLAG and pCMV-T7, the fragment encoding one copy of the FLAG epitope or the fragment encoding one copy of the T7 epitope was inserted into pCMV vector, respectively. Several mutant cDNAs encoding WNK1, WNK4, SPAK, OSR1, NKCC1-(1–289), NKCC2-(1–181), or NCC were generated by polymerase chain reaction and subcloned into the pCMV-FLAG, pCMV-T7, pGEX4T-1, or pGEX4T-3 as indicated. The accuracy of all clones was verified by DNA sequencing.

Yeast Two-hybrid Screening and MS/MS Analysis—Full-length human WNK1 was fused to the GAL4 DNA-binding domain, and yeast two-hybrid screening was performed as described (26). LC-MS/MS analysis was performed as described previously (27). Briefly, FLAG-WNK1 was expressed in HEK293 cells and immunoprecipitated by anti-FLAG antibody. The immunocomplexes were eluted with a FLAG peptide and then digested with *Achromobacter* protease I, and the resulting peptides were analyzed using a nanoscale LC-MS/MS system.

Antibodies—Antibody to WNK1 was generated with a peptide corresponding to the N-terminal 18 amino acids of human WNK1. Anti-SPAK/OSR1 antibody was prepared by immunizing rabbits with a keyhole limpet hemocyanin-conjugated synthetic peptide (RAKKVRRVPGSSG, amino acids 362–374 of human SPAK and amino acids 314–326 of human OSR1). Anti-phospho OSR1 polyclonal antibody was produced in rabbit by immunizing with a keyhole limpet hemocyanin-conjugated synthetic phosphopeptide corresponding to residues 319–332 of OSR1 (RRVPGS (pS) GRLHKTE). The serum was affinity-purified with phosphopeptide- and the non-phosphopeptide-conjugated cellulose. Monoclonal antibodies against FLAG and T7 were purchased from Sigma and Novagen, respectively.

Immunoprecipitation and Immunoblotting—HEK293 and MDCK cells were cultured in Dulbecco's modified Eagle's medium with standard supplements. HEK293 cells were transfected with the indicated plasmids by the calcium phosphate precipitation method at 50–80% confluence. After 24 h after transfection, cells were lysed in 1% Triton X-100 lysis buffer (50 mM Tris-HCl, pH 7.5, 150 mM NaCl, 1 mM EGTA, 1 mM EDTA, 1% Triton X-100, 1 mM orthovanadate, 50 mM sodium fluoride, 1 mM phenylmethylsulfonyl fluoride, 1 μg/ml aprotinin, 1 mM dithiothreitol, 0.27 M sucrose). Protein complexes were immunoprecipitated with the indicated antibodies according to standard procedures. Isolated protein complexes were separated by SDS-PAGE and transferred to polyvinylidene fluoride membranes (Hybond-P, Amersham Biosciences). Blots were probed with the indicated antibodies, and bound antibodies were visualized using horseradish peroxidase-conjugated secondary antibodies (Amersham Biosciences) and Western Lightning chemiluminescence reagent Plus (PerkinElmer Life Sciences) according to standard procedures. For ^{32}P labeling, transfected cells were incubated for 6 h with [^{32}P]phosphate (1 mCi/ml) and then lysed as described above.

Expression of GST-tagged Fusion Proteins in Escherichia coli—The pGEX constructs were transformed into *E. coli* BL21 cells, and a 0.5-liter culture was grown at 37 °C to an A_{600} of 0.8. Isopropyl-D-galactosidase was added to final 0.2 mM to induce protein expression, and the cells were cultured for another 16 h at 20 °C. Cells were harvested by centrifugation and lysed by freeze-thawing and sonication in 1% Triton X-100 lysis buffer. Glutathione *S*-transferase (GST)-tagged proteins were puri-

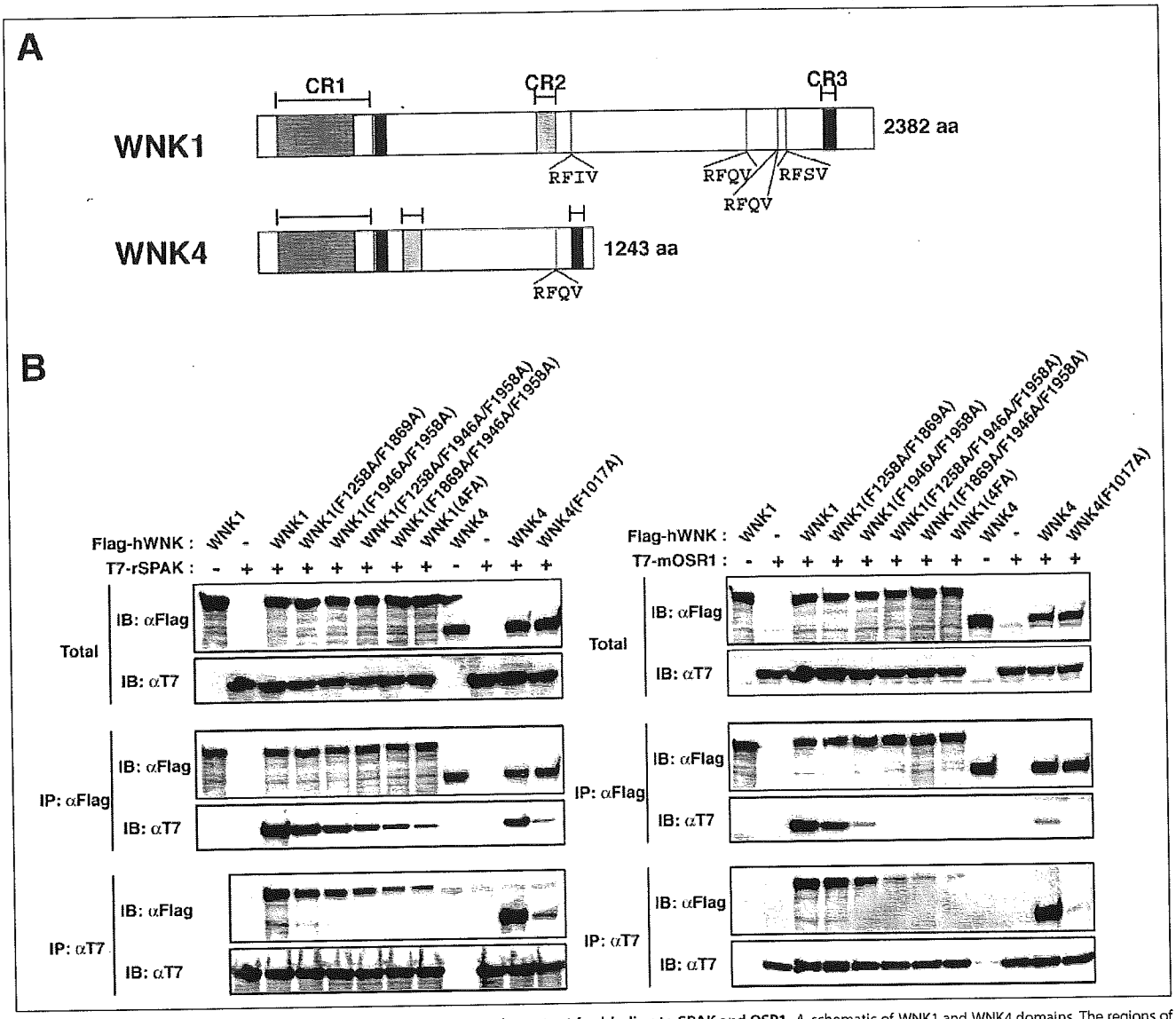

FIGURE 2. **The putative SPAK-binding motifs within WNK kinases are important for binding to SPAK and OSR1.** *A*, schematic of WNK1 and WNK4 domains. The regions of conserved homology, CR1 (kinase domain), CR2, and CR3, are indicated by *horizontal bars* above each protein. The locations of putative SPAK-binding motifs consisting of the consensus sequence (R/K-F-X-V/I) are indicated by *vertical bars*. *B*, T7-tagged rat SPAK (*left*) and mouse OSR1 (*right, mOSR1*) were co-transfected with various WNK1 and WNK4 mutants as indicated. Protein complexes were co-immunoprecipitated (*IP*) using either T7 antibody (*αT7*) or FLAG antibody (*αFLAG*) and then immunoblotted (*IB*) with αT7 or αFLAG. *hWNK*, human WNK.

fied from the lysates using glutathione-Sepharose and eluted from the resin in 10 mM glutathione.

Kinase Assays—Immunoprecipitated and GST-protein complexes were incubated in a kinase buffer containing 50 mM Tris-HCl, pH 7.5, 10 mM $MgCl_2$, and 100 μM [γ-^{32}P]ATP (2 μCi). After incubation for 30 min at 30 °C, the reactions were terminated by the addition of SDS sample buffer, and the proteins were separated by SDS-PAGE. Substrate phosphorylation was analyzed by autoradiography and an image analyzer (Fujix BAS 2500). For determination of phosphorylation sites by MS/MS, GST-SPAK(KM) was incubated with WNK1-(1–665) in a buffer containing 1 mM ATP for 6 h. Solutions used in hypotonic stress experiments were as follows. Basic medium contained 135 mM NaCl, 5 mM KCl, 1 mM $CaCl_2$/$MgCl_2$, 1 mM Na_2HPO_4/Na2SO4, and 15 mM sodium HEPES, pH 7.4. Low Cl^- hypotonic medium contained 67.5 mM sodium gluconate, 2.5 mM potassium gluconate, 0.5 mM $CaCl_2$/$MgCl_2$, 1 mM Na_2HPO_4/Na_2SO_4, and 7.5 mM sodium HEPES, pH 7.4.

RESULTS

Identification of the STE20-related Kinases SPAK and OSR1 as WNK1-associated Molecules—To identify a protein(s) that physically associates with WNK1, we employed two strategies: yeast two-hybrid screening and FLAG tag immunoprecipitation assays coupled with LC-MS/MS analysis. Several positive clones and putative binding proteins were identified, including STE20-like kinase SPAK. As SPAK was identified by both approaches, we analyzed it further. To investigate whether endogenous SPAK is associated with WNK1 in living cells, we generated antibodies to a peptide of SPAK (the sequence is a 100% match of the corresponding sequence of OSR1, a kinase closely related to SPAK) and a peptide of human WNK1. The anti-SPAK/OSR1 antibody reacted with three bands of 62, 60, and 58 kDa in HEK293 cell extracts and with two bands of 62 and 58 kDa in MDCK cell extracts (Fig. 1). The specificity of anti-SPAK/OSR1 antibody was confirmed by the competition